university of groningen

Implementing the 1D and 2D Conservation Element/Solution Element scheme coupled with the Van der Waals model

Frank Westers

March, 2017

Bachelor thesis

Physics

University of Groningen

Supervisor 1: Dr. T.L.C. Jansen

Supervisor 2: Dr. T.A. Schlathölter

External Supervisor: Dr. M. Parsani

Abstract

The CE/SE scheme is a fast and accurate method for solving flow problems. The current version of the scheme depends on the perfect gas law, which works fine for atmospheric pressures, but breaks down at higher pressures. The aim of this thesis was to change the CE/SE scheme such that it depends on the Van der Waals equation of state instead. This new algorithm should be able to simulate dense gas flows with higher precision. Next, this was going to be used to simulate flows around a wing profile and to explore the differences between the perfect gas law and the Van der Waals gas law. In this thesis, the NACA-0012 wing profile is used, because a lot of experimental data is available for this airfoil and it is widely used in throughout literature to test the precision of new algorithms.

For 1D, the results were promising and the CE/SE method was able to calculate the Sod Shock tube with much higher accuracy compared to the original CE/SE scheme.

For the 2D case, two different algorithms have been written, one using a structured mesh and one using an unstructured mesh. The structured mesh has been validated using Brown and Argrow (1998) and matched visually very well. The unstructured mesh also gave visually correct results for a wave on a 30 degree wedge, but failed to calculate the flow around the wing profile properly. Possible causes have been listed, which can be used in further research on this topic. This thesis presents the theoretical background and a 1D and 2D implementation of the Van der Waals CE/SE scheme for structured grids.

Contents

List of Symbols

Greek symbols

α	Van der Waals force parameter
δ	$\frac{\bar{R}}{\bar{c}_v}$
γ	Constant specific heat ratio
ρ	Density

Latin symbols

a	Speed of sound
b	Van der Waals covolume parameter
c_v	Constant heat ratio at constant volume
E	Total energy per unit mass
e	Internal energy per unit mass
p	Pressure
R	Specific gas constant
T	Temperature
t	Time coordinate
u	Velocity in x-direction
x	Spatial coordinate
Z	Compressibility factor

subscripts

c	Value at critical point

1. Introduction

1.1 Background

For ages, there has been a clear way of doing science: first, a certain phenomenon was being observed. Based on the observations, someone creates a model and tests if the predictions of the model are correct. Based on these tests, the model is adapted to give more accurate results. This goes on until a model explains the observed phenomenon well enough. Very quickly, however, models became too complex to calculate by hand. Only very simple cases could be addressed using these models. For complex cases, a more simple model would be applied for analysis. The rise of computers changed this drastically. It became possible to do larger computations than ever before. New algorithms were designed for solving complex equations, and an entirely new branch of physics came into existence: computational physics.

The above story has been particularly true for fluid physics. In the 19th century, the Navier-Stokes equation and the Euler equation were derived, which describe the motion of viscous and non-viscous fluids. Only for a few simple cases, these equations can be solved analytically. For more complex geometries, it has to be solved be solved numerically. The field of physics concerned with numerically analyzing the physics of fluids is called computational fluid dynamics (CFD).

In 1995, a new method for numerically solving the Navier-Stokes and Euler equation in 1 dimension was proposed by Sin-Chung Chang in Chang (1995). This new algorithm was called Conservation Element Solution Element (CE/SE). The algorithm was extended to 2 dimensions a few years later in Chang et al. (1999) and it has proven to be a useful method for simulating fluid flows. Initially, the solver has been implemented using a perfect gas. In this research project, the perfect gas in the CE/SE scheme will be replaced by a gas that obeys the Van der Waals equation of state in one dimension and two dimensions. The goal is to explore whether

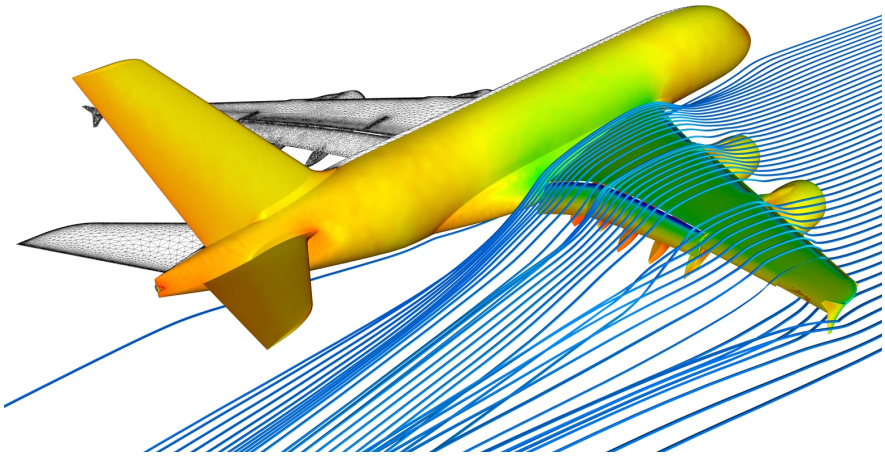

Figure 1.1: One of the applications of fluid dynamics is finding optimal wing profiles

using a more complex model results in higher accuracy than using the simple, perfect gas equation. Special attention will be paid to detecting non-classical gas phenomena. The inviscid flow over a NACA-0012 airfoil, a backward step and a 30-degree wedge will be used as test cases for this. These test cases have been chosen, because validated and published results are available. Specifically, the NACA-0012 wing profile is widely used throughout literature to validate and test the precision of new algorithms.

1.2 Objectives

- Implement the Van der Waals equation of state in the one and two dimensional CE/SE scheme for solving the Euler equations
- Explore the differences in the outcome of the CE/SE scheme for a perfect gas and a Van der Waals gas in 1 dimension and two dimensions.

1.3 Structure of the Report

In the next chapter, the existing literature on the topic will be discussed. The rest of reports starts with introducing and deriving the mathematical tools that are required in the rest of the report. This includes derivations of several thermodynamic quantities as well as the nondimen-

sionalization scheme. In the next chapters, the CE/SE scheme will be explained in 1D as well as 2D. For each dimension, the equations that are dependent of the EOS used are determined, and the differences between the perfect gas and Van der Waals version are calculated. In chapter 6, several test cases in 1D and 2D will be presented, and the differences in outcome between the perfect gas and Van der Waals gas are explored. Chapter 7 summarizes the conclusions of this comparison and makes recommendations for future work.

2. Literature Survey

Chang (1995) was the first to describe the Conservation Element Solution Element algorithm in 1995. Since then, it has been extended to more dimensions and improved by using different geometries, for example in Chang et al. (1999). A C++ implementation was described in Shen et al. (2015). This implementation will be the starting point for the implementation of the Van der Waals CE/SE scheme. Next, Chang et al. (1998) provides a more systematic and clear explanation of the CE/SE method. This technical memorandum will be the main source for understanding the scheme in more depth.

Next, Arina (2004) and Aldo and Argrow (1995) are used for obtaining the required equations regarding the Van der Waals equation of state and the nondimsionalization scheme.

After the Van der Waals model has been implemented, it must be validated to ensure the correctness of the data. For the one-dimensional case, this will be done by comparing it to a paper written by Argrow (1996) in 1996. In this paper, dense gas shock tube flows have been analyzed, using the Van der Waals model and the TVDM scheme for various initial states. As the results in this paper also show non-classical phenomena, it is a great way for testing the implementation of the Van der Waals CE/SE scheme in 1D.

In 2D, Brown and Argrow (1998) will be used for validating the code created in this project. The set-up of the article is similar to Argrow (1996): the two-dimensional Euler equations are solved using the Van der Waals model coupled with a scheme called PCTVD. It analyses perfect gas results and dense gas results, with a focus non-classical behavior. Favale and Gadda (2013) and Cinnella and Congedo (2005) will be used to validate the flow around the NACA-0012 wing profile.

3. Derivation of useful quantities

3.1 The nondimensionalization scheme

This project makes use dimensionless variables. There are two reasons for choosing this approach. First, the nondimensionalization scheme can be chosen in such a way that the equation of state is independent of the gas, which makes the algorithm more convenient to use and understand. A second reason for using dimensionless numbers is to be consistent with other literature on this topic, which all use this approach. Many ways exist to make variables dimensionless, but to be able to validate the results, a scheme similar to the one used in Argrow (1996) will be used. In this scheme, all variables are made dimensionless using only length of the shock tube $\bar{L}$, specific gas constant $\bar{R}$, the critical pressure $\bar{p}_c$, critical density $\bar{\rho}_c$ and critical temperature $\bar{T}_c$ of the gas. The paper by Argrow (1996) contains a small error its definition of the dimensionless time coordinate. It uses $t = \frac{\bar{L}\bar{t}}{\sqrt{\bar{R}\bar{T}_c}}$, which results in t having a unit in seconds squared. The scheme used in this project fixes this and can be found in table 3.1. Everywhere in the thesis, dimensional variables will be denoted with a bar on top of the symbol.

Property	**Nondimensionalization**		**Property**	**Nondimensionalization**
Pressure	$p = \frac{\bar{p}}{\bar{p}_c}$		Density	$\rho = \frac{\bar{\rho}}{\bar{\rho}_c}$
Temperature	$T = \frac{\bar{T}}{\bar{T}_c}$		Velocity	$u = \frac{\bar{u}}{\sqrt{\bar{R}\bar{T}_c}}$
Internal Energy	$e = \frac{\bar{e}}{\bar{R}\bar{T}_c}$		Heat capacity constant volume	$\delta = \frac{\bar{R}}{\bar{c}_v} = \gamma - 1$
Van der Waals covolume parameter	$b = \bar{b}\bar{\rho}_c$		Van der Waals force parameter	$\alpha = \frac{\bar{\alpha}\bar{\rho}_c}{\bar{R}\bar{T}_c}$
Space coordinate	$x = \frac{\bar{x}}{\bar{L}_x}$		Time coordinate	$t = \frac{\bar{t}\sqrt{\bar{R}\bar{T}_c}}{\bar{L}}$

Table 3.1:
The nondimensionalization scheme

3.2 Perfect gas

A perfect gas is a gas that obeys the ideal gas law $\bar{p} = \bar{\rho}\bar{R}\bar{T}$. In this thesis, a perfect gas is a synonym for a calorically perfect gas. This means that the heat capacity is assumed to be constant and the internal energy per unit mass is given by $\bar{e} = \bar{c}_v\bar{T}$, with c_v being the molar heat capacity at constant volume. Next, the total energy per unit mass is defined as the internal energy plus the kinetic energy: $E = e + \frac{1}{2}u^2$. Combining these equations enables us to derive equations 3.1 to 3.4, which turn out to be useful later in the project.

$$\begin{aligned} e\bar{R}\bar{T}_c &= \frac{\bar{R}}{\delta}T\bar{T}_c \\ \Rightarrow \qquad e &= \frac{T}{\delta} \end{aligned} \tag{3.1}$$

$$\begin{aligned} E\bar{R}\bar{T}_c &= \bar{R}\bar{T}_c e + \frac{1}{2}\left(u\sqrt{\bar{R}\bar{T}_c}\right)^2 \\ \Rightarrow \qquad E &= e + \frac{1}{2}u^2 \end{aligned} \tag{3.2}$$

$$\begin{aligned} p\bar{p}_c &= \rho\bar{\rho}_c\bar{R}T\bar{T}_c \\ \Rightarrow \qquad p &= \frac{\bar{\rho}\bar{R}\bar{T}_c}{\bar{p}_c}\rho T = \rho T \qquad (3.3) \\ &= \rho\delta(E - \frac{1}{2}u^2) \qquad (3.4) \end{aligned}$$

In these equations, $\delta = \frac{\bar{R}}{\bar{c}_v}$. From $\bar{c}_p - \bar{c}_v = \bar{R}$, it follows immediately that $\delta = \gamma - 1$. Lastly, the speed of sound is given by the Newton-Laplace equation:

$$a = \sqrt{\frac{K_s}{\rho}} = \sqrt{\gamma\frac{p}{\rho}} \tag{3.5}$$

3.3 Van der Waals gas

The same way as perfect gas is described by the ideal gas law, a Van der Waals gas is described by the Van der Waals equation of state. This project uses the notation which is used in Arina (2004):

$$\bar{p} = \frac{\bar{R}\bar{T}\bar{\rho}}{1-\bar{b}\bar{\rho}} - \bar{\alpha}\bar{\rho}^2 \tag{3.6}$$

where α and b are the so-called Van der Waals constants, which are dependent of the type of gas. α is a factor to correct for the inter-molecular forces within a gas and the b corrects for the size of the molecules $r > 0$. During the nondimensionalization process, both constants disappear and the final equation is independent of the type of gas. Their dimensional values are given in Arina (2004) by $\bar{\alpha} = \frac{27}{64}\frac{\bar{R}_c^2\bar{T}_c^2}{\bar{p}_c}$ and $\bar{b} = \frac{\bar{R}\bar{T}_c}{8\bar{p}_c}$. Also, this project assumes a constant heat capacity and hence, $\bar{e} = \bar{c}_v\bar{T} - \bar{\alpha}\bar{\rho}$. This equation differs slightly from the definition used in Argrow (1996), which claims $\bar{e} = \bar{c}_v\bar{T} - \bar{\alpha}\bar{\rho}^2$. A quick dimensional analysis shows that this equation cannot be correct. This is most likely a typographical error, as the derivatives of this equation in the paper are correct.

For a Van der Waals gas, the total energy is the same as for a perfect gas: $\bar{E} = \bar{e} + \frac{1}{2}\bar{u}^2$. Finally, one last new quantity is introduced, namely the critical compressibility factor $Z_c = \frac{\bar{p}_c}{\bar{\rho}_c\bar{R}\bar{T}_c}$. To derive the value of this factor, its individual values must be expressed in terms of α and b first.

$$\bar{R}\bar{T}_c = \frac{\bar{R}^2\bar{T}_c^2}{\bar{R}\bar{T}_c} = \frac{\frac{64}{27}\bar{p}_c\bar{\alpha}}{8\bar{p}_c\bar{b}} = \frac{8\bar{\alpha}}{27\bar{b}}$$

$$\bar{p}_c = \frac{\bar{p}_c^2}{\bar{p}_c} = \frac{\frac{R^2\bar{T}_c^2}{64\bar{b}^2}}{\frac{27}{64}\frac{R^2\bar{T}_c^2}{\bar{\alpha}}} = \frac{\bar{\alpha}}{27\bar{b}^2}$$

So now:

$$\frac{\bar{\alpha}}{27\bar{b}^2} = \frac{\frac{8\bar{\alpha}}{27\bar{b}}\bar{\rho}_c}{1-\bar{b}\bar{\rho}_c} - \bar{\alpha}\bar{\rho}_c^2$$

$$\Rightarrow \qquad \bar{\rho}_c = \frac{1}{3\bar{b}}$$

Now, we can derive a value for the critical compressibility Z_c:

$$Z_c = \frac{\bar{p}_c}{\bar{\rho}_c \bar{R} \bar{T}_c} = \frac{\frac{\bar{\alpha}}{27\bar{b}^2}}{\frac{1}{3\bar{b}} \frac{8\bar{\alpha}}{27\bar{b}}} = \frac{3}{8} \tag{3.7}$$

It follows that

$$\begin{aligned} \alpha \frac{\bar{R}\bar{T}_c}{\bar{\rho}_c} &= \frac{27}{64} \frac{\bar{R}^2 \bar{T}_c^2}{p_c} \\ \Rightarrow \qquad \alpha &= \frac{27}{64} \frac{1}{Z_c} = \frac{9}{8} \end{aligned} \tag{3.8}$$

$$\begin{aligned} \frac{b}{\bar{\rho}_c} &= \frac{\bar{R}\bar{T}_c}{8\bar{p}_c} \\ \Rightarrow \qquad b &= \frac{1}{8Z_c} = \frac{1}{3} \end{aligned} \tag{3.9}$$

Hence, the Van der Waals counterparts for equations 3.1 to 3.4 are:

$$\begin{aligned} e\bar{R}\bar{T}_c &= \frac{\bar{R}}{\delta} T \bar{T}_c - \alpha \frac{\bar{R}\bar{T}_c}{\bar{\rho}_c} \rho \bar{\rho}_c \\ \Rightarrow \qquad e &= \frac{T}{\delta} - \alpha\rho \end{aligned} \tag{3.10}$$

$$\begin{aligned} E\bar{R}\bar{T}_c &= e\bar{R}\bar{T}_c + \frac{1}{2}\left(v\sqrt{\bar{R}\bar{T}_c}\right)^2 \\ \Rightarrow \qquad E &= e + \frac{1}{2}u^2 \end{aligned} \tag{3.11}$$

$$\begin{aligned} p\bar{p}_c &= \frac{\rho\bar{\rho}_c \bar{R} T \bar{T}_c}{1 - \frac{1}{3\bar{\rho}_c}\rho\bar{\rho}_c} - \frac{9}{8}\frac{\bar{R}\bar{T}_c}{\bar{\rho}_c}(\rho\bar{\rho}_c)^2 \\ \Rightarrow \qquad p &= \frac{3\rho T}{3-\rho}\frac{1}{Z_c} - \frac{9}{8}\frac{1}{Z_c}\rho^2 \\ &= \frac{8\rho T}{3-\rho} - 3\rho^2 \end{aligned} \tag{3.12}$$

Using equation 3.10 and 3.11

$$\begin{aligned} p &= \frac{8\rho\delta(e+\frac{9}{8}\rho)}{3-\rho} - 3\rho^2 \\ &= \frac{\rho\delta(8E-4u^2+9\rho)}{3-\rho} - 3\rho^2 \end{aligned} \tag{3.13}$$

3.3.1 Speed of sound

Because Aldo and Argrow (1995) and Argrow (1996) disagree on the equation for the speed of sound, it will be derived again in this section, to be sure that the correct equation is being used. We start with the generic equation for the speed of sound, which is valid for any equation of state (Arina (2004)):

$$\bar{a} = \sqrt{\frac{\bar{p}}{\bar{\rho}^2}\left(\frac{\partial\bar{p}}{\partial\bar{e}}\right)_{\bar{\rho}} + \left(\frac{\partial\bar{p}}{\partial\bar{\rho}}\right)_{\bar{e}}} \tag{3.14}$$

It should be noted that Arina (2004) uses $\frac{p}{\bar{\rho}^2}$ instead of $\frac{\bar{p}}{\bar{\rho}^2}$. This is most likely a typo, as using the non-dimensionalized pressure does not lead to any reasonable equation for the speed of sound. Also, this dimensionless value for the pressure is not mentioned anywhere else in the section. Taking $\bar{p}$ instead of p leads to the following equation of the speed of sound:

$$a = \sqrt{\frac{4}{9}\left[(1+\delta)\frac{4T}{3-\rho} - \rho)\right]} \tag{3.15}$$

See appendix A for the derivation of this formula.

3.4 Euler equation

3.4.1 One-dimensional Euler equation

The motion of a gas can be derived from three conservation laws: the conservation of mass, momentum and energy. Conservation of mass means that the mass inside a closed volume V can only change by a flow of mass through the borders of the volume. The same applies for momentum and energy. Mathematically, these conservation laws in 1 dimension are described

by the Euler equation:

$$\frac{\partial \mathbf{U}}{\partial t} + \frac{\partial \mathbf{F}}{\partial x} = 0 \tag{3.16}$$

U represents the property which is conserved (mass, momentum or energy) and **F** is the output flux of this property along the border of the volume. Since a positive change in, for example, mass is completely caused by a negative change in output flux, both quantities have to be equal. Three Euler equations can be derived: one for the density ρ, one for the momentum ρv and one for the energy E. This leads to the following set of equations, as derived in Dullemond and Kuiper (2015).

$$\frac{\partial}{\partial \bar{t}} \begin{bmatrix} \bar{\rho} \\ \bar{\rho}\bar{u} \\ \bar{\rho}\bar{E} \end{bmatrix} + \frac{\partial}{\partial \bar{x}} \begin{bmatrix} \bar{\rho}\bar{u} \\ \bar{\rho}\bar{u}^2 + \bar{p} \\ (\bar{\rho}\bar{E} + \bar{p})\bar{u} \end{bmatrix} = 0 \tag{3.17}$$

The dimensional Euler equation is independent of the equation of state, however, as will be shown shortly, the dimensionless one is not. Each conserved property will be discussed individually below to obtain its dimensionless value.

Conservation of mass

$$\begin{aligned} \frac{\partial \bar{\rho}}{\partial \bar{t}} + \frac{\partial(\bar{\rho}\bar{u})}{\partial \bar{x}} &= 0 \\ \frac{\partial(\rho\bar{\rho}_c)}{\partial(t\frac{\bar{L}}{\sqrt{\bar{R}\bar{T}_c}})} + \frac{\partial(\rho\bar{\rho}_c u\sqrt{\bar{R}\bar{T}_c})}{\partial(x\bar{L})} &= 0 \\ \frac{\bar{\rho}_c\sqrt{\bar{R}\bar{T}_c}}{\bar{L}}\left[\frac{\partial \rho}{\partial t} + \frac{\partial(\rho u)}{\partial x}\right] &= 0 \\ \frac{\partial \rho}{\partial t} + \frac{\partial(\rho u)}{\partial x} &= 0 \end{aligned} \tag{3.18}$$

Conservation of momentum

$$\begin{aligned}
\frac{\partial(\bar{\rho}\bar{u})}{\partial\bar{t}} + \frac{\partial}{\partial\bar{x}}(\bar{\rho}\bar{u}^2 + \bar{p}) &= 0 \\
\frac{\partial(\rho\bar{\rho}_c u\sqrt{\bar{R}\bar{T}_c})}{\partial(t\frac{\bar{L}}{\sqrt{\bar{R}\bar{T}_c}})} + \frac{\partial}{\partial(x\bar{L})}[\rho\bar{\rho}_c(u\sqrt{\bar{R}\bar{T}_c})^2 + p\bar{p}_c] &= 0 \\
\frac{\bar{\rho}_c\bar{R}\bar{T}_c}{\bar{L}}\Big[\frac{\partial(\rho u)}{\partial t} + \frac{\partial}{\partial x}(\rho u^2 + p\frac{p_c}{\bar{\rho}_c\bar{R}\bar{T}_c})\Big] &= 0 \\
\frac{\partial(\rho u)}{\partial t} + \frac{\partial}{\partial x}(\rho u^2 + Z_c p) &= 0
\end{aligned} \tag{3.19}$$

Conservation of energy

$$\begin{aligned}
\frac{\partial(\bar{\rho}\bar{E})}{\partial\bar{t}} + \frac{\partial}{\partial\bar{x}}\big[(\bar{\rho}\bar{E} + \bar{p})\bar{u}\big] &= 0 \\
\frac{\partial(\rho\bar{\rho}_c E\bar{R}_s\bar{T}_c)}{\partial(t\frac{\bar{L}}{\sqrt{\bar{R}\bar{T}_c}})} + \frac{\partial}{\partial(x\bar{L})}\big[(\rho\bar{\rho}_c E\bar{R}_s\bar{T}_c + p\bar{p}_c)(u\sqrt{\bar{R}\bar{T}_c})\big] &= 0 \\
\frac{\bar{\rho}_c(\bar{R}_s\bar{T}_c)^{\frac{3}{2}}}{\bar{L}}\Big\{\frac{\partial(\rho E)}{\partial t} + \frac{\partial}{\partial x}\big[(\rho E + p\frac{\bar{p}_c}{\bar{\rho}_c\bar{R}_s\bar{T}_c})u\big]\Big\} &= 0 \\
\frac{\partial(\rho E)}{\partial t} + \frac{\partial}{\partial x}\big[(\rho E + Z_c p)u\big] &= 0
\end{aligned} \tag{3.20}$$

Combining these results into the nondimensional Euler equation gives:

$$\frac{\partial}{\partial t}\begin{bmatrix}\rho\\ \rho u\\ \rho E\end{bmatrix} + \frac{\partial}{\partial x}\begin{bmatrix}\rho u\\ \rho u^2 + Z_c p\\ (\rho E + Z_c p)u\end{bmatrix} = 0 \tag{3.21}$$

This result can also be obtained more readily by noting that the output flux f_m equals the conserved property times the velocity, e.g. $f_1 = \rho u = u_1 u$. This is canceled out by the variables of differentiation because a dimensional analysis shows that the unit of tu is equal to x. Therefore the dimensionless Euler equation is equal to the dimensional one, except by the term Z_c in front of p. It should be noted that the term Z_c depends on the equation of state (EOS) that is used.

For a perfect gas $Z_c = 1$ and for a Van der Waals gas $Z_c = \frac{3}{8}$. Therefore, the dimensionless Euler equation depends on the EOS it is applied to.

3.4.2 One-dimensional Jacobian matrix of the Euler equation

First, consider the Euler equation, rewritten in a more compact form:

$$\frac{\partial u_m}{\partial t} + \frac{\partial f_m}{\partial x} = 0, \text{ where } m = 1,2,3 \tag{3.22}$$

where u_1, u_2 and u_3 are $\rho, \rho u$ and ρE respectively. Similarly, f_1, f_2 and f_3 are ρu, $(\rho u^2 + Z_c p)$ and $(\rho E + Z_c p)u$. f_m depends completely on u_m and therefore the Euler equation can be rewritten in a form which consists of only the variables u_m, $m = 1,2,3$. Since the equation for expressing the pressure in terms of u_m is different for a perfect gas than for a Van der Waals gas, two versions of the equation appear. For a perfect gas, using equation 3.4, it becomes:

$$u_1 = \rho \qquad u_2 = \rho u \qquad u_3 = E \tag{3.23}$$

$$f_1 = u_2 \qquad f_2 = \delta u_3 + \frac{(2-\delta)(u_2)^2}{2u_1} \qquad f_3 = (\delta+1)\frac{u_2 u_3}{u_1} - \frac{\delta(u_2)^3}{2(u_1)^2} \tag{3.24}$$

And for a Van der Waals gas:

$$u_1 = \rho \qquad u_2 = \rho u \qquad u_3 = E \tag{3.25}$$

$$f_1 = u_2 \qquad f_2 = \frac{(u_2)^2}{u_1} + Z_c p_{vdw} \qquad f_3 = (u_3 + Z_c p_{vdw})\frac{u_2}{u_1} \tag{3.26}$$

where

$$p_{vdw} = \frac{u_1 \delta (8u_3 - 4\left(\frac{u_2}{u_1}\right)^2 + 9u_1)}{3 - u_1} - 3(u_1)^2 \tag{3.27}$$

Now, we can define the 3x3 Jacobian matrix **A**, with the elements given by:

$$f_{m,k} = \frac{\partial f_m}{\partial u_k}, \text{ where } m,k = 1,2,3 \tag{3.28}$$

This Jacobian matrix is key in understanding the CE/SE scheme. Its derivation for a perfect gas and a Van der Waals gas can be found in appendix A.

3.4.3 Multi-dimensional Euler equation

The Euler equation in multiple dimensions has been derived in Dullemond and Kuiper (2015) and is given by the three conservation laws in tensor form, where i and k denote the N-dimensional space component:

$$\begin{aligned}
\partial_{\bar{t}}\ \bar{\rho} + \sum_{\bar{i}} \partial_{\bar{i}}\ (\bar{\rho}(\bar{u_i})) &= 0 \\
\partial_{\bar{t}}\ (\bar{\rho}(\bar{u_i})) + \sum_{\bar{k}} \partial_{\bar{k}}\ (\bar{\rho}(\bar{u_k})(\bar{u_i}) + \delta_{\bar{i}\bar{k}}\bar{p}) &= 0 \\
\partial_{\bar{t}}\ (\bar{\rho}\bar{E}) + \sum_{\bar{i}} \partial_{\bar{i}}\ \left[(\bar{\rho}\bar{E} + \bar{p})(\bar{u_i})\right] &= 0
\end{aligned}$$

In 2 dimensions, this results in the following equation:

$$\frac{\partial}{\partial \bar{t}} \begin{bmatrix} \bar{\rho} \\ \bar{\rho}\bar{u} \\ \bar{\rho}\bar{v} \\ \bar{\rho}\bar{E} \end{bmatrix} + \frac{\partial}{\partial \bar{x}} \begin{bmatrix} \bar{\rho}\bar{u} \\ \bar{\rho}\bar{u}^2 + \bar{p} \\ \bar{\rho}\bar{u}\bar{v} \\ (\bar{\rho}\bar{E} + \bar{p})\bar{u} \end{bmatrix} + \frac{\partial}{\partial \bar{y}} \begin{bmatrix} \bar{\rho}\bar{v} \\ \bar{\rho}\bar{v}\bar{u} \\ \bar{\rho}\bar{v}^2 + \bar{p} \\ (\bar{\rho}\bar{E} + \bar{p})\bar{v} \end{bmatrix} = 0 \tag{3.29}$$

Using table 3.1 to nondimensionalize the equations results in the following dimensionless conservation laws:

Conservation of mass

$$\begin{aligned}
\partial_{\bar{t}}\ \bar{\rho} + \sum_{\bar{i}} \partial_{\bar{i}}\ (\bar{\rho}(\bar{u_i})) &= 0 \\
\partial_{\left[t\frac{\bar{L}}{\sqrt{\bar{R}\bar{T}_c}}\right]}\ (\rho\bar{\rho}_c) + \sum_{\bar{i}} \partial_{[i\bar{L}]}\ (\rho\bar{\rho}_c(u_i\sqrt{\bar{R}\bar{T}_c})) &= 0 \\
\frac{\bar{\rho}_c\sqrt{\bar{R}\bar{T}_c}}{\bar{L}}\left[\partial_t\ \bar{\rho} + \sum_i \partial_i\ (\rho u_i)\right] &= 0 \\
\partial_t\ \rho + \sum_i \partial_i\ (\rho u_i) &= 0
\end{aligned} \tag{3.30}$$

Conservation of momentum

$$\begin{aligned}
\partial_{\bar{t}}\left(\bar{\rho}\bar{u}_i\right)+\sum_{\bar{k}}\partial_{\bar{k}}\left(\bar{\rho}\bar{u}_k\bar{u}_i+\delta_{ik}\bar{p}\right)&=0\\
\partial_{\left[t\frac{\bar{L}}{\sqrt{\bar{R}\bar{T}_c}}\right]}\left(\rho\bar{\rho}_c u_i\sqrt{\bar{R}\bar{T}_c}\right)+\sum_{\bar{k}}\partial_{[k\bar{L}]}\left(\rho\bar{\rho}_c u_k u_i\left(\sqrt{\bar{R}\bar{T}_c}\right)^2+\delta_{ik}p\bar{p}_c\right)&=0\\
\frac{\bar{\rho}_c\bar{R}\bar{T}_c}{\bar{L}}\left[\partial_t\left(\rho u_i\right)+\sum_k\partial_k\left(\rho u_k u_i+\delta_{ik}p\frac{\bar{p}_c}{\bar{R}\bar{T}_c\bar{\rho}_c}\right)\right]&=0\\
\partial_t\left(\rho u_i\right)+\sum_k\partial_k\left(\rho u_k u_i+\delta_{ik}Z_c p\right)&=0
\end{aligned}\tag{3.31}$$

Along each axis i

Conservation of energy

$$\begin{aligned}
\partial_{\bar{t}}\left(\bar{\rho}\bar{E}\right)+\sum_{\bar{i}}\partial_{\bar{i}}\left[\left(\bar{\rho}\bar{E}+\bar{p}\right)\bar{u}_i\right]&=0\\
\partial_{\left[t\frac{\bar{L}}{\sqrt{\bar{R}\bar{T}_c}}\right]}\left(\rho\bar{\rho}_c E\bar{R}\bar{T}_c\right)+\sum_{\bar{i}}\partial_{[i\bar{L}]}\left[\left(\rho\bar{\rho}_c E\bar{R}\bar{T}_c+p\bar{p}_c\right)u_i\sqrt{\bar{R}\bar{T}_c}\right]&=0\\
\frac{\left(\bar{\rho}_c\bar{R}\bar{T}_c\right)^{\frac{3}{2}}}{\bar{L}}\left[\partial_t\left(\rho E\right)+\sum_i\partial_i\left[\left(\rho E+p\frac{\bar{p}_c}{\bar{\rho}_c\bar{R}\bar{T}_c}\right)u_i\right]\right]&=0\\
\partial_t\left(\rho E\right)+\sum_i\partial_i\left[\left(\rho E+Z_c p\right)u_i\right]&=0
\end{aligned}\tag{3.32}$$

And again, in 2 dimensions, this leads to

$$\frac{\partial}{\partial t}\begin{bmatrix}\rho\\ \rho u\\ \rho v\\ \rho E\end{bmatrix}+\frac{\partial}{\partial x}\begin{bmatrix}\rho u\\ \rho u^2+Z_c p\\ \rho uv\\ (\rho E+Z_c p)u\end{bmatrix}+\frac{\partial}{\partial y}\begin{bmatrix}\rho v\\ \rho vu\\ \rho v^2+Z_c p\\ (\rho E+Z_c p)v\end{bmatrix}=0\tag{3.33}$$

3.4.4 Multi-dimensional Jacobian matrices of the Euler equation

Now that the Euler equation has been extended to more dimensions, it is also possible to find the multi-dimensional counterpart of the 1D Jacobian matrix, which has been defined in section 3.4.2. We first write the N-dimensional Euler equation in the same notation as in section 3.4.2:

$$\frac{\partial u_m}{\partial t} + \sum_i \frac{\partial f_m^i}{\partial x} = 0, \qquad m = 1,2,3,4 \tag{3.34}$$

As before, the superscript i denotes the dimensional space component of the flux. Now, for an N-dimensional system, N Jacobian matrices $\mathbf{A}^i$ of size $(2+N)$x$(2+N)$ can be defined, consisting of the elements:

$$(f_{m,k})^i = \frac{\partial f_m^i}{\partial u_k} \qquad m,k = 1,2,3,4 \tag{3.35}$$

So, for 2 dimensions, the two 4x4 matrices $\mathbf{A}^x$ and $\mathbf{A}^y$, with dimensional space components x and y, have the elements:

$$f_{m,k}^x = \frac{\partial f_m^x}{\partial u_k} \qquad\qquad f_{m,k}^y = \frac{\partial f_m^y}{\partial u_k}, \qquad\qquad m,k = 1,2,3,4 \tag{3.36}$$

These matrices are explicitly given in appendix A

4. The one dimensional CE/SE scheme

4.1 The marching scheme

In the year 1995, S.C. Chang published a paper which described a new method for numerically solving flow problems containing shocks, rarefaction waves and much more types of waves that were hard to solve accurately using the existing techniques. The new method was called conservation element solution element (CE/SE). The development of the technique was guided by the belief that it should focus on the use of the original integral form of conservation laws, instead of the differential form. The differential form is based on the assumption that the solution is smooth, which makes it hard to capture a numerical solution in regions where this assumption is not valid, such as in shocks. Two important design principles were that the method should enforce local as well as global flux conservation in space and time and that space and time should always be treated on equal footing. These principles will become clearer during the discussion of the method in this section. More design principles and what drove the development of the scheme can be found in Chang (1995).

This explanation will use the Euler equation in fluid dynamics to explain the working of the CE/SE scheme. However, it can also be applied to the Navier-Stokes equations and other initial-value problems with similar differential equations. Now, consider the generalized Euler equation in one dimension:

$$\frac{\partial \mathbf{U}}{\partial t} + \frac{\partial \mathbf{F}}{x} = \frac{\partial}{\partial t}\begin{bmatrix} u_1 \\ u_2 \\ u_3 \end{bmatrix} + \frac{\partial}{\partial x}\begin{bmatrix} f_1 \\ f_2 \\ f_3 \end{bmatrix} = \frac{\partial u_m}{\partial t} + \frac{\partial f_m}{\partial x} = 0,\ m = 1,2,3$$

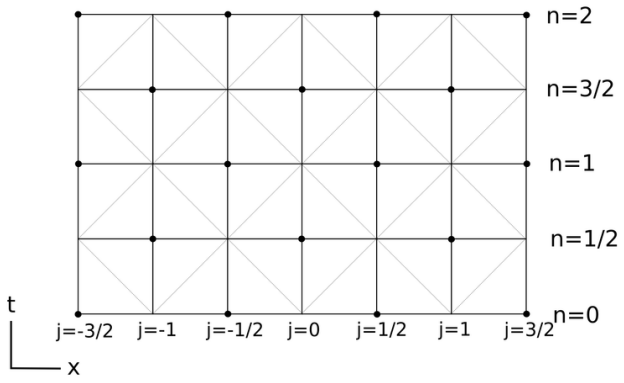

Figure 4.1: CE/SE mesh

where **U** is the conserved variables and **F** the flux in terms of u_m, $m = 1,2,3$. For the rest of this section, m will always be taken to run from 1 to 3. This partial differential equation (PDE) is a consequence of a more general conservation law and follows under the assumption that the derivatives exists at all points. This general law is written as an integral over the conserved region $S(V)$ (Chang et al. (1998)):

$$\oint_{S(V)} \vec{h}_m \cdot d\vec{s} = 0 \tag{4.1}$$

where $\vec{h}_m = \langle f_m, u_m \rangle$.

Also, consider a two dimensional space-time Euclidean space E_2, with space on one axis and time on the other. In this space, let let Ω denote all the mesh points (j,n), with $(2n) \in \mathbb{Z}$ and $(j+n+\frac{1}{2}) \in \mathbb{Z}$, as shown in figure 4.1. j and n respresent the spatial and time coordinate respectively. Each mesh point is surrounded by the solution element (SE), whose borders are shown in figure 4.1 by the dashed lines. For any $(x,t) \in SE(j,n)$, $u(x,t)$ and $f(x,t)$ can be approximated by the first-order Taylor expansion at position (x,y):

$$u_m^*(x,t;j,n) = (u_m)_j^n + (u_{mx})_j^n (x - x_j) + (u_{mt})_j^n (t - t^n) \tag{4.2}$$

$$f_m^*(x,t;j,n) = (f_m)_j^n + (f_{mx})_j^n (x - x_j) + (f_{mt})_j^n (t - t^n) \tag{4.3}$$

In this equation, $(u_m)_j^n$ is the value of u_m at mesh position (j,n). $(u_{mx})_j^n$ and $(u_{mt})_j^n$ are the spatial and time derivative of $(u_m)_j^n$ respectively. f_m is given in equation 3.21 and $(f_{mx})_j^n$ and $(f_{mt})_j^n$ are its spatial and time derivatives. x_j and t^n are the spatial and time coordinate of (j,n)

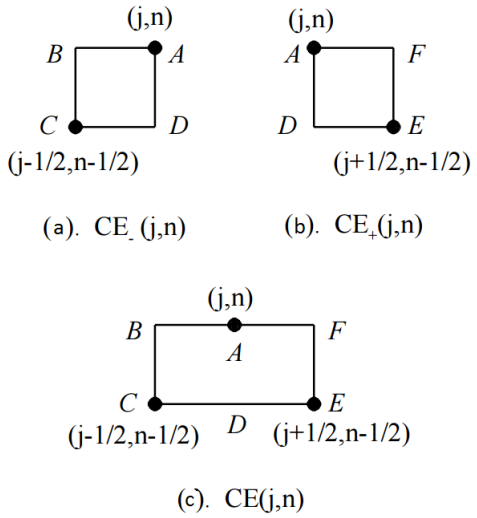

Figure 4.2: The conservation elements (Edited from figure 4 in Chang et al. (1998)

respectively. Similar toequation 4.1, we define:

$$\vec{h}_m^* = \left\langle f_m^*(x,t;j,n), u_m^*(x,t;j,n) \right\rangle \tag{4.4}$$

Now, let E_2 be divided into rectangles where two of the four corners are elements in Ω. These rectangles are enclosed by the solid lines in figure 4.1. The rectangle that has element (j,n) as the upper right vertex is called $CE_-(j,n)$ and the one having (j,n) as the upper-left vertex is called $CE_+(j,n)$, as shown in figure 4.2. Together they are called the conservation element, CE. Because equation 4.1 is true for any volume and equation 4.4 approximates the values of u_m and f_m at any point within the SE, it follows that

$$\oint_{S(CE_\pm(j,n))} \vec{h}_m^* \cdot d\vec{s} = 0 \tag{4.5}$$

To solve this integral, it should be noted that each $CE_\pm$ consists of 4 sides, of which 2 lie in $SE(j,n)$ and the other 2 in $SE(j \pm \frac{1}{2}, n - \frac{1}{2})$. Therefore, we know the flux through the bottom and the sides of the CE and we can combine equation 4.2, 4.3 with 4.1 to derive the value for the mesh points at time $t = n$ using the values of the mesh points at time $t = n - \frac{1}{2}$. Plugging

equation 4.2 and 4.3 into equation 4.5 results in: (Chang et al. (1998) section 2.3)

$$(u_m)_j^n - (u_m)_{j\pm1/2}^{n-1/2} \pm \frac{\Delta x}{4}\left[(u_{mx})_{j\pm\frac{1}{2}}^{n-\frac{1}{2}} + (u_{mx})_j^n)\right] \\ \pm \frac{\Delta t}{\Delta x}\left[(f_m)_{j\pm\frac{1}{2}}^{n-\frac{1}{2}} - (f_m)_j^n\right] \pm \frac{(\Delta t)^2}{4\Delta x}\left[(f_{mt})_{j\pm\frac{1}{2}}^{n-\frac{1}{2}} + (f_{mt})_j^n\right] = 0 \tag{4.6}$$

In the same paper it is shown that this can be rewritten into matrix form:

$$\left[(\mathbf{I}\mp\mathbf{A}^+)\vec{u} \pm (\mathbf{I}\mp(\mathbf{A}^+)^2)\frac{\Delta x}{4}(\vec{u}_x)\right]_j^n = \left[(\mathbf{I}\mp\mathbf{A}^+)\vec{u} \mp (\mathbf{I}\mp(\mathbf{A}^+)^2)\frac{\Delta x}{4}(\vec{u}_x)\right]_{j\pm\frac{1}{2}}^{n-\frac{1}{2}} \tag{4.7}$$

Here $\mathbf{I}$ is the identity matrix, $\mathbf{A}^+ = \frac{\Delta t}{\Delta x}\mathbf{A}$, $\mathbf{A}$ is the Jacobian defined by 3.28 and $\vec{u}_j^n$ is the 3x1 matrix formed by u_m with $m = 1,2,3$. Now we have two unknowns ($\vec{u}_j^n$ and $(\vec{u}_x)_j^n$) and the two equations (one for + and one for − in equation 4.7). If we now define:

$$(\vec{s}_\pm)_{j\pm\frac{1}{2}}^{n-\frac{1}{2}} = \left[\vec{u} \mp (\mathbf{I}\pm\mathbf{A}^+)\frac{\Delta x}{4}(\vec{u}_x)\right]_{j\pm\frac{1}{2}}^{n-\frac{1}{2}} \tag{4.8}$$

equation 4.7 can be solved for $\vec{u}_j^n$ and written as:

$$\vec{u}_j^n = \frac{1}{2}\left\{\left[(\mathbf{I}-\mathbf{A}^+)\vec{s}_+\right]_{j+\frac{1}{2}}^{n-\frac{1}{2}} + \left[(\mathbf{I}+\mathbf{A}^+)\vec{s}_-\right]_{j-\frac{1}{2}}^{n-\frac{1}{2}}\right\} \tag{4.9}$$

Equation 4.9 is the first part of the marching scheme in the CE/SE algorithm. If the scheme is implemented in a computer program, it is often easier to use the non-matrix form:

$$(u_m)_j^n = \frac{1}{2}\left[(u_m)_{j-1/2}^{n-1/2} + (u_m)_{j+1/2}^{n-1/2} + (s_m)_{j-1/2}^{n-1/2} + (s_m)_{j+1/2}^{n-1/2}\right] \tag{4.10}$$

with

$$(s_m)_j^n = \frac{\Delta x}{4}(u_{mx})_j^n + \frac{\Delta t}{\Delta x}(f_m)_j^n + \frac{(\Delta t)^2}{4\Delta x}(f_{mt})_j^n, \quad m = 1,2,3 \tag{4.11}$$

and

$$(f_m)_j^n = \sum_{k=1}^{3}(f_{m,k})_j^n(u_k)_j^n \tag{4.12}$$

$$(f_{mt})_j^n = -\mathbf{A}(u_{mt})_j^n \tag{4.13}$$

If equation 4.7 is solved for $(\vec{u}_x)_j^n$, one obtains the second part in the marching scheme. We first define

$$(\vec{S}_\pm)_j^n = \left[(\mathbf{I} \mp \mathbf{A}^+)_j^n\right]^{-1}\left[(\mathbf{I} \mp \mathbf{A}^+)\,\vec{u} \mp (\mathbf{I} \mp (\mathbf{A}^+)^2)\,\vec{u}_x\right]_{j\pm\frac{1}{2}}^{n-\frac{1}{2}} \tag{4.14}$$

and solving 4.7 for $(\vec{u}_x)_j^n$ gives:

$$(\vec{u}_x)_j^n = \frac{1}{2}(\vec{S}_+ - \vec{S}_-)_j^n \tag{4.15}$$

As the definition of $\vec{S}_\pm$ involves a matrix inversion, we have to make sure that the inverse exists. In Appendix A, section A.4, it is shown that it exists if the Courant number is smaller than 1. Therefore Δt should always be chosen in such a way that the CFL-condition $\frac{(u+a)\Delta t}{\Delta x} \leq C_{max} = 1$ is satisfied. From a physical point of view, this inequality can be understood in the following way: Imagine Δx to be very small and Δt to be very large. At time n, we measure a wave at spatial position j. Because Δt is large, the wave will have passed multiple grid points at time $n+\Delta t$. However, to calculate the wave at its new spatial position, we have only access to the data of its neighbors at the previous time step. Since the wave was multiple grid points away in the previous time step, these neighbors do not contain any information about the wave at time n and a calculation of the wave at time $n+\Delta t$ is impossible. Therefore, Δt should be chosen such, that it the wave will pass one grid point away at maximum. That is, Δt must be smaller than the difference in distance between the grid points divided by the speed of information, $(\frac{\Delta x}{u+a})$.

The equation for u_{mx} which is used in this paper is derived in Chang et al. (1998), section 2.7 and is a simplification of the $a-\epsilon-\alpha-\beta$ scheme, which tries increase the precision of the calculations by adding several constants. To simplify these calculations, these constant can be chosen in such a way such a way that the scheme reduces to just one parameter. This makes the scheme more compatible with parallel computing, while it is still able to accurately capture shocks. To understand the scheme, let us first define:

$$(\vec{u}_{x\pm})_j^n = \pm\frac{1}{2}\left(\vec{u}_{j\pm\frac{1}{2}}^{\,n-\frac{1}{2}} + \frac{\Delta t}{2}(\vec{u}_t)_{t\pm\frac{1}{2}}^{\,n-\frac{1}{2}} - \vec{u}_j^n\right) \tag{4.16}$$

Simply taking the average of $(\vec{u}_{x+})_j^n$ and $(\vec{u}_{x-})_j^n$ would give valid results for $(u_{mx})_j^n$ only if no discontinuities occur. At a discontinuity, $(j-\frac{1}{2},n)$ and $(j+\frac{1}{2},n)$ lie at the opposite sides of the boundary and hence, simply taking the average is not enough. Therefore, the result must be smoothened by taking a biased average:

$$W_0(x_-,x_+,\alpha)=\frac{|x_+|^\alpha x_- + |x_-|^\alpha x_+}{|x_+|^\alpha + |x_-|^\alpha}, \text{ with } (|x_+|^\alpha + |x_-|^\alpha) > 0 \tag{4.17}$$

$$\vec{u}_{x_j}^n = W_0((\vec{u}_{x+})_j^n, (\vec{u}_{x-})_j^n, \alpha) \tag{4.18}$$

The outcome of equation 4.17 will be biased towards the lowest value between x_- and x_+, for $\alpha > 0$. In a smooth area, $(\vec{u}_{x+})_j^n$ and $(\vec{u}_{x-})_j^n$ will lie close together, and the outcome of W_0 will be close to the regular central average. However, at a discontinuity, the difference between the input values of W_0 will be large. Since the input consists of the derivatives of u, a low value of $(\vec{u}_{x\pm})_j^n$ means a smooth area in u. Therefore, the average is biased towards the smooth region, that is, the lowest value. This effect only occurs on the mesh points lying on the discontinuty and does not effect the mesh points in a smooth area. This is one of the advantages of the CE/SE scheme.

To conclude, the CE/SE marching scheme consists of two equations, one for advancing to $(u_m)_j^n$ and another one for calculating $(u_{mx})_j^n$. Therefore, given $(u_m)_{j\pm\frac{1}{2}}^{n-\frac{1}{2}}$ and $(u_{mx})_{j\pm\frac{1}{2}}^{n-\frac{1}{2}}$, the next time level can be calculated as follows:

$$(u_{mt})_j^n = -\mathbf{A}(u_{mx})_j^n \tag{4.19}$$

$$(f_m)_j^n = \sum_{k=1}^{3} (f_{m,k})_j^n (u_k)_j^n \tag{4.20}$$

$$(f_{mt})_j^n = \mathbf{A}(u_{mt})_j^n \tag{4.21}$$

$$(s_m)_j^n = \frac{\Delta x}{4}(u_{mx})_j^n + \frac{\Delta t}{\Delta x}(f_m)_j^n + \frac{(\Delta t)^2}{4\Delta x}(f_{mt})_j^n, \;\; m=1,2,3 \tag{4.22}$$

$$(u_{mx\pm})_j^n = \frac{2}{\Delta x}\left((u_m)_j^n - (u_m)_{j\pm\frac{1}{2}}^{n-\frac{1}{2}} - \Delta t(u_{mt})_{j\pm\frac{1}{2}}^{n-\frac{1}{2}}\right) \tag{4.23}$$

And the marching scheme is:

$$(u_m)_j^n = \frac{1}{2}\left[(u_m)_{j-1/2}^{n-1/2} + (u_m)_{j+1/2}^{n-1/2} + (s_m)_{j-1/2}^{n-1/2} + (s_m)_{j+1/2}^{n-1/2}\right] \tag{4.24}$$

$$(u_{mx})_j^n = W_0((u_{mx+})_j^n, (u_{mx-})_j^n, \alpha) \tag{4.25}$$

4.2 Perfect & Van der Waal gas differences

All existing implementations of the CE/SE algorithm, such as in Shen et al. (2015) and Chena et al. (2011), make use of the perfect gas law, as described in section 3.2. If the perfect gas law is replaced by the Van der Waals equation of state, the basic structure of the algorithm as described in section 4.1 does not change, as no reference to any EOS has been made in this section. Equation 4.19 - 4.25 show that the only required input to advance from time step $n-\frac{1}{2}$ to n, is the Jacobian $\mathbf{A}$. This matrix is based on the Euler equation as defined in equation 3.23 - 3.26, which does depend on the definition of the pressure as a function of ρ, u and E and hence, on the equation of state. Therefore, the first difference between the perfect gas and the Van der Waals version of the CE/SE scheme is the Jacobian matrix. The definition of the matrix for both the perfect and the Van der Waals gas can be found in Appendix A. In Appendix A, section A.4 it shown that the condition for the inversion of $(\mathbf{I} \mp \mathbf{A}^+)_j^n$ does not change. Secondly, the CFL condition depends on the speed of sound, which, as shown in chapter 3, does also depend on the equation of state. Therefore, to ensure that the CFL condition is not violated, the equation for the speed of sound must be updated according to the Van der Waals model.

5. The two dimensional CE/SE scheme

5.1 The marching scheme

The marching scheme in two dimensions shows a lot of similarities with the scheme in one dimension. Therefore, this chapter will have the same structure as chapter 4.

As in chapter 4, we start by considering the Euler equation in differential and integral form:

$$\frac{\partial \mathbf{U}}{\partial t}+\frac{\partial \mathbf{F}^x}{x}+\frac{\partial \mathbf{F}^y}{y} = \frac{\partial}{\partial t}\begin{bmatrix}u_1\\u_2\\u_3\\u_4\end{bmatrix}+\frac{\partial}{\partial x}\begin{bmatrix}f_1^x\\f_2^x\\f_3^x\\f_4^x\end{bmatrix}+\frac{\partial}{\partial y}\begin{bmatrix}f_1^y\\f_2^y\\f_3^y\\f_4^y\end{bmatrix} = \frac{\partial u_m}{\partial t}+\frac{\partial f_m^x}{\partial x}+\frac{\partial f_m^y}{\partial y} = 0,\ m=1,2,3,4$$

which can be derived from

$$\oint_{S(V)} \vec{h}_m \cdot d\vec{s} = 0,\ m=1,2,3,4 \tag{5.1}$$

where $\vec{h}_m = \langle f_m^x, f_m^y, u_m \rangle$, by using Gauss's Divergence theorem. For the rest of this chapter, the subscript $_m$ runs from 1 to 4, unless stated otherwise.

Now, let us define a uniform three dimensional space-time Euclidean space E_3. The first versions of the CE/SE scheme were based on triangular meshes, but this was later extended to quadrilateral meshes. The derivation for the CE/SE scheme using triangular meshes can be found in Appendix B. This chapter will explain the CE/SE scheme using the less complex quadrilateral mesh, also because this mesh is used in Shen et al. (2015), which provides the base code for the Van der Waals code. Figure 5.1a shows the layout of the mesh. The white circles represent the mesh points at time step $n \in \mathbb{Z}$ and the white triangles represent mesh points at time $n+\frac{1}{2}$. A mesh point at spatial coordinate (i, j) at time step n is denoted by $P_{i,j}^n$. The SE of $P_{i-1/2,j-1/2}^{n-1/2}$ is shown in figure 5.1b. The CE of a point $P_{i,j}^n$ consists of 4 cuboids, as shown in 5.1c. 5.1d shows

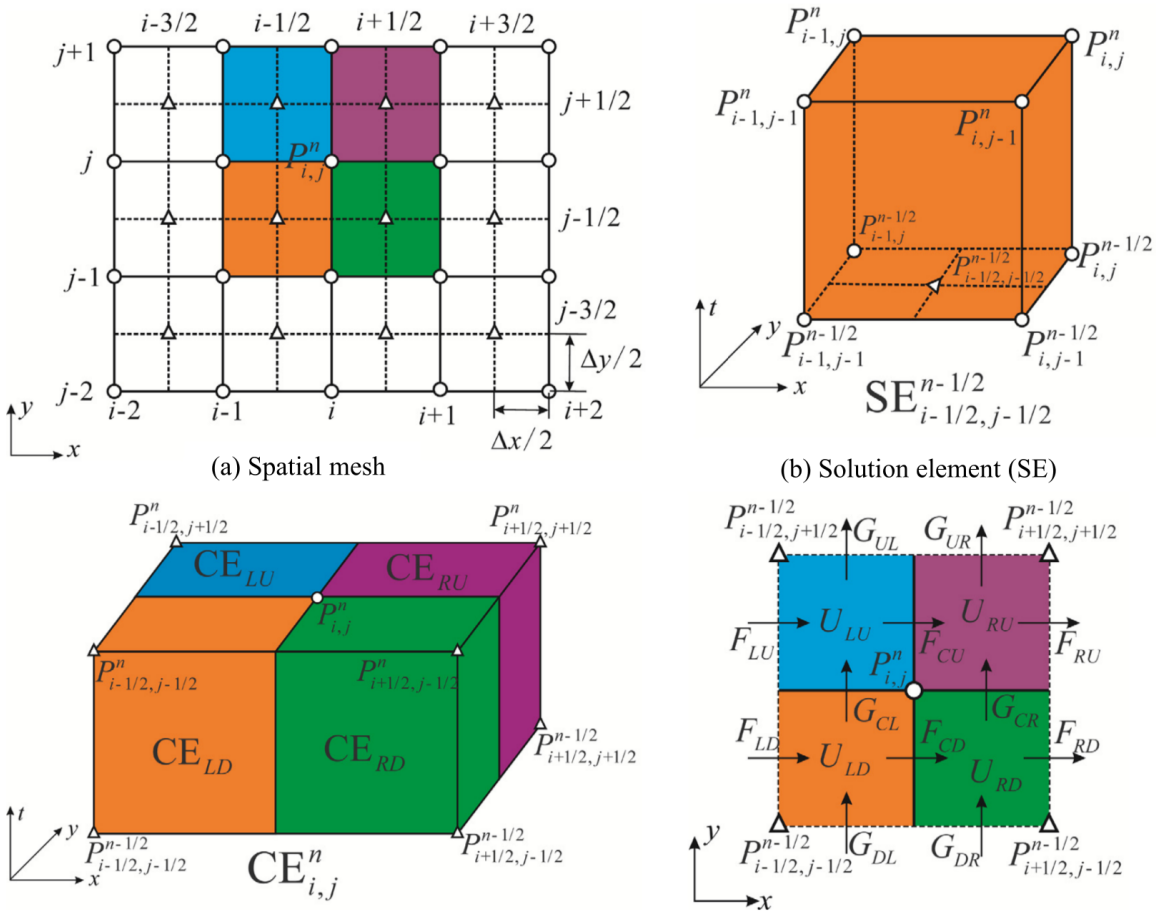

Figure 5.1: The definition of the CE and SE in 2D[1]

a top view of the CE and names all the fluxes flowing in and out the of the CEs. It can be seen that the boundary of the CE of $P^n_{i,j}$ is formed by subsets of SEs of the previous time step, namely, $P^{n-1/2}_{i-1/2,j-1/2}$, $P^{n-1/}_{i+1/2,j-1/2}$, $P^{n-1/2}_{i-1/2,j+1/2}$ and $P^n_{i+1/2,j+1/2}$. This ensures that a mesh point at time step n can be calculated based on the neighboring mesh points at time step $n-\frac{1}{2}$.

Using the same notation as in the previous chapters, the values of $u^n_{i,j}$ and $f^n_{i,j}$ can be approximated by the first-order Taylor expansion around (i,j):

$$u^*_m(x,y,t;j,k,t) = (u_m)^n_{(i,j)} + (u_{mx})^n_{(i,j)}(x-x_{(i,j)}) + (u_{my})^n_{(i,j)}(y-y_{(i,j)}) + (u_{mt})^n_{(i,j)}(t-t^n) \quad (5.2)$$

$$f^{x*}_m(x,y,t;j,k,t) = (f^x_m)^n_{(i,j)} + (f^x_{mx})^n_{(i,j)}(x-x_{(i,j)}) + (f^x_{my})^n_{(i,i)}(y-y_{(i,j)}) + (f^x_{mt})^n_{(i,j)}(t-t^n) \quad (5.3)$$

$$f^{y*}_m(x,y,t;j,k,t) = (f^y_m)^n_{(i,j)} + (f^y_{mx})^n_{(i,j)}(x-x_{(i,j)}) + (f^y_{my})^n_{(i,j)}(y-y_{(i,j)}) + (f^y_{mt})^n_{(i,j)}(t-t^n) \quad (5.4)$$

[1]This image is an copy-edit based on figure 2 in Shen et al. (2015).

Here f_m^x and f_m^y are the fluxes in the x- and y-direction. These equations are used to define $\vec{h}_m^* = \langle f_m^{x*}, f_m^{y*}, u_m^* \rangle$, which enables us to approximate the solution for eq. 5.1. Solving this integral, leads to the following four equations (Shen et al. (2015)):

$$(\vec{U}_{LD})_{i,j}^n = \Big[\vec{u} - \vec{u}_x \frac{\Delta x}{4} - \vec{u}_y \frac{\Delta y}{4} \Big]_{i,j}^{n-1/2} = \Big[\vec{U}_{LD} + (\vec{F}_{LD} - \vec{F}_{CD}) \frac{\Delta t}{\Delta x} + (\vec{G}_{DL} - \vec{G}_{CL}) \frac{\Delta t}{\Delta y} \Big]_{i,j}^{n-1/2} \tag{5.5}$$

$$(\vec{U}_{RD})_{i,j}^n = \Big[\vec{u} + \vec{u}_x \frac{\Delta x}{4} - \vec{u}_y \frac{\Delta y}{4} \Big]_{i,j}^{n-1/2} = \Big[\vec{U}_{RD} + (\vec{F}_{CD} - \vec{F}_{RD}) \frac{\Delta t}{\Delta x} + (\vec{G}_{DR} - \vec{G}_{CR}) \frac{\Delta t}{\Delta y} \Big]_{i,j}^{n-1/2} \tag{5.6}$$

$$(\vec{U}_{RU})_{i,j}^n = \Big[\vec{u} + \vec{u}_x \frac{\Delta x}{4} + \vec{u}_y \frac{\Delta y}{4} \Big]_{i,j}^{n-1/2} = \Big[\vec{U}_{RU} + (\vec{F}_{CU} - \vec{F}_{RU}) \frac{\Delta t}{\Delta x} + (\vec{G}_{CR} - \vec{G}_{UR}) \frac{\Delta t}{\Delta y} \Big]_{i,j}^{n-1/2} \tag{5.7}$$

$$(\vec{U}_{LU})_{i,j}^n = \Big[\vec{u} - \vec{u}_x \frac{\Delta x}{4} + \vec{u}_y \frac{\Delta y}{4} \Big]_{i,j}^{n-1/2} = \Big[\vec{U}_{LU} + (\vec{F}_{LU} - \vec{F}_{CU}) \frac{\Delta t}{\Delta x} + (\vec{G}_{CL} - \vec{G}_{UL}) \frac{\Delta t}{\Delta y} \Big]_{i,j}^{n-1/2} \tag{5.8}$$

The notation is consistent with figure 5.1. That is, $\vec{U}_{LD}$ is the total value of u_m in CE_{LD}, $\vec{F}_{LD}$ is the flux flowing into CE_{LD} in the x-direction, etc. This formula can be understood intuitively in the following way: The value of, for example, U_{LD} equals the value of the previous time step, plus the inflow minus outflow of the conserved property. As can be seen in figure B.1ad, the inflow in the x-direction is $\frac{\Delta t}{\Delta x}\vec{F}_{LD}$ and the outflow $\frac{\Delta t}{\Delta x}\vec{F}_{CD}$. In the y-direction, the inflow is $\frac{\Delta t}{\Delta y}\vec{G}_{DL}$ and the outflow $\frac{\Delta t}{\Delta y}\vec{G}_{CL}$. Adding this together leads to equation 5.5. The same applies for the other CEs. Adding equation 5.5-5.8 , leads to a equation for $u_{i,j}^n$:

$$\vec{u}_{i,j}^n = \frac{1}{4}\Big[\vec{U}_{LD} + \vec{U}_{RD} + \vec{U}_{RU} + \vec{U}_{LU} + \frac{\Delta t}{\Delta x}\big(\vec{F}_{LD} + \vec{F}_{LU} - \vec{F}_{RD} - \vec{F}_{RU}\big) + \frac{\Delta t}{\Delta y}\big(\vec{G}_{DL} + \vec{G}_{DR} - \vec{G}_{UL} - \vec{G}_{UR}\big) \Big]_{i,j}^{n-1/2} \tag{5.9}$$

For the spatial derivatives, one can derive multiple solutions, because the number of equations in greater than the number of unknowns. For $\vec{u}_x$, this results in:

$$\big(\vec{u}_x^D\big)_{i,j}^n = \frac{2}{\Delta x}\Big[\vec{U}_{RD} - \vec{U}_{LD} + \frac{2\Delta t}{(\Delta x)^2}\big(2\vec{F}_{CD} - \vec{F}_{LD} - \vec{F}_{RD}\big) + \frac{2\Delta t}{\Delta y \Delta x}\big(\vec{G}_{DR} - \vec{G}_{CR} - \vec{G}_{DL} + \vec{G}_{CL}\big) \Big]_{i,j}^{n-1/2} \tag{5.10}$$

$$\big(\vec{u}_x^U\big)_{i,j}^n = \frac{2}{\Delta x}\Big[\vec{U}_{RU} - \vec{U}_{LU} + \frac{2\Delta t}{(\Delta x)^2}\big(2\vec{F}_{CU} - \vec{F}_{LU} - \vec{F}_{RU}\big) + \frac{\Delta t}{\Delta y \Delta x}\big(\vec{G}_{CR} - \vec{G}_{UR} - \vec{G}_{CL} + \vec{G}_{UL}\big) \Big]_{i,j}^{n-1/2} \tag{5.11}$$

and solving for $\vec{u}_y$ leads to

$$\left(\vec{u}_y^L\right)_{i,j}^n = \frac{2}{\Delta y}\left[\vec{U}_{LU} - \vec{U}_{LD} + \frac{\Delta 2t}{\Delta x \Delta y}\left(\vec{F}_{LU} - \vec{F}_{CU} - \vec{F}_{LD} + \vec{F}_{CD}\right) + \frac{2\Delta t}{(\Delta y)^2}\left(2\vec{G}_{CL} - \vec{G}_{DL} - \vec{G}_{UL}\right)\right]_{i,j}^{n-1/2} \tag{5.12}$$

$$\left(\vec{u}_y^R\right)_{i,j}^n = \frac{2}{\Delta y}\left[\vec{U}_{RU} - \vec{U}_{RD} + \frac{\Delta 2t}{\Delta x \Delta y}\left(\vec{F}_{CU} - \vec{F}_{RU} - \vec{F}_{CD} + \vec{F}_{RD}\right) + \frac{2\Delta t}{(\Delta y)^2}\left(2\vec{G}_{CR} - \vec{G}_{DR} - \vec{G}_{UR}\right)\right]_{i,j}^{n-1/2} \tag{5.13}$$

In this derivation, it is assumed that the CFL condition is satisfied, which, in 2D is given by:

$$\frac{u_x \Delta t}{\Delta x} + \frac{u_y \Delta t}{\Delta y} \leq C_{max} = 1 \tag{5.14}$$

All that is left is finding an equation for calculating the fluxes in the x- and y-direction. These equations are similar to the ones for calculating U: the flux is equal to the flux in the previous time step plus the incoming flux, plus the incoming flux in the orthogonal direction plus the flux that was created over time. This leads to the following equation (only one equation for each direction is given, the others can easily be derived using figure 5.1d)

$$F_{LD} = \left(\vec{f}^x - \vec{f}_y^x \frac{\Delta y}{4} - \vec{f}_t^x \frac{\Delta t}{4}\right) \tag{5.15}$$

$$G_{DL} = \left(\vec{f}^y - \vec{f}_x^y \frac{\Delta y}{4} - \vec{f}_t^y \frac{\Delta t}{4}\right) \tag{5.16}$$

where f^x and f^y denote the total flux in the x- and y-direction respectively. f^x and f^y are calculated in the same way as in the 1D case, using the Jacobian $\mathbf{A}$. Only now we need two Jacboians: one for x-direction, $\mathbf{A}^x = \frac{\partial f_m^x}{\partial u_k}$, and one for the y-direction $\mathbf{A}^y = \frac{\partial f_m^y}{\partial u_k}$. Hence

$$\vec{f}_x^x = \mathbf{A}^x \vec{u}_x \qquad \vec{f}_x^y = \mathbf{A}^y \vec{u}_x \qquad \vec{f}_y^x = \mathbf{A}^x \vec{u}_y \qquad \vec{f}_y^y = \mathbf{A}^y \vec{u}_y \tag{5.17}$$

Just as in the previous section, we can take the arithmetic average of the two solutions for the spatial derivatives, but this will give incorrect results at discontinuities. Therefore we define

$$(u_{mx})_{i,j}^n = W_0\left(\left[\left(u_{mx}^L\right)_{i,j}^n, \left(u_{mx}^U\right)_{i,j}^n, \alpha\right)\right. \qquad \text{and} \qquad (\vec{u}_y)_{i,j}^n = W_0\left(\left(u_{mx}^L\right)_{i,j}^n, \left(u_{mx}^R\right)_{i,j}^n, \alpha\right) \tag{5.18}$$

Now we have derived all the equations to advance to time step $t + \frac{1}{2}$.

5.2 Perfect & Van der Waal gas differences

Just as in the 1D case, no explicit reference to any equation has been made in the previous section. The only two variables depending on the EOS are the Jacobian $\mathbf{A}$ and the speed of sound a, which is required for satisfying the CFL-condition. Therefore the updates to convert the scheme to use the Van der Waals model are similar to the ones in the 1D case.

6. Comparison of the two EOS

This chapter will explore the real gas effects in various 1D and 2D test cases. The CE/SE scheme in combination with the perfect gas law has already been implemented in Shen et al. (2015) and the Van der Waals version of the scheme was implemented for this thesis. To decrease the probability of having bugs in the new code, it will be tested against known solutions. Once the validation is completed, new test cases will be run to see the difference in outcome between perfect gas and Van der Waals gases.

6.1 The one-dimensional case

6.1.1 Validation

Argrow (1996) will be used to validate the 1D Van der Waals CE/SE scheme. This paper states the result of 3 dense shock tube test cases, which are listed in table 6.1. The results of the new VdW CE/SE solver have been plotted next in the same graph as the results obtained by Argrow (1996). These graphs are shown in figure 6.1. As can be seen, the results match visually very well, which make it likely that the Van der Waals model has been implemented correctly. It should be noted

Case	δ	CFL	t_{end}	Gases
1D1	0.0125	0.8	0.1807	$(\rho, v, p) = \begin{cases} (1.818,\ 0\ , 3.0) & 0 \leq x \leq 0.5 \\ (0.275,\ 0\ , 0.575) & 0.5 < x \leq 1 \end{cases}$
1D2	0.0125	0.8	0.4801	$(\rho, v, p) = \begin{cases} (0.879,\ 0\ , 1.090) & 0 \leq x \leq 0.5 \\ (0.562,\ 0\ , 0.885) & 0.5 < x \leq 1 \end{cases}$
1D3	0.0125	0.8	0.2917	$(\rho, v, p) = \begin{cases} (0.879,\ 0\ , 1.090) & 0 \leq x \leq 0.5 \\ (0.275,\ 0\ , 0.575) & 0.5 < x \leq 1 \end{cases}$

Table 6.1: The intial conditions for the four test cases

however, that the graphs of Argrow (1996) have been extracted using third-party software. Since the paper was old, it was hard to reconstruct the numerical data from the paper. This explains the low amount of data points. Therefore a more precise validation is impossible.

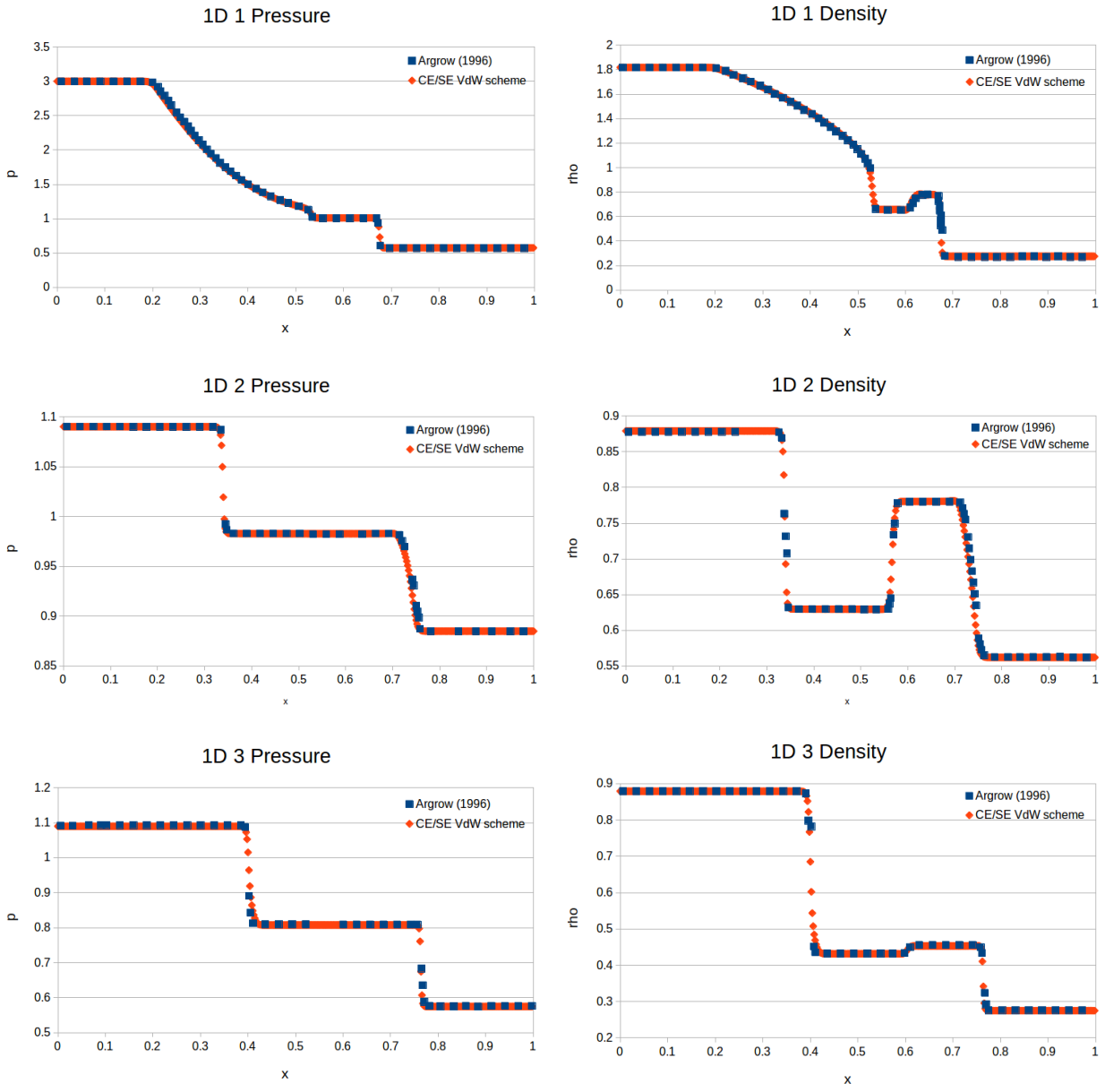

Figure 6.1: Validation of the 1D Van der Waals CE/SE scheme

6.1.2 Analysis of results

Let us recall perfect gas law and the Van der Waals equation of state:

$$\text{Perfect gas law:} \qquad \bar{p} = \bar{\rho}\bar{R}\bar{T} \tag{6.1}$$

$$\text{Van der Waals EOS:} \qquad \bar{p} = \frac{\bar{R}\bar{T}\bar{\rho}}{1-\bar{b}\bar{\rho}} - \bar{\alpha}\rho^2 \tag{6.2}$$

It can be seen that the Van der Waals models approaches the perfect gas model as ρ approaches zero. Therefore, 3 test cases will be examined, which all have a different pressure and density, to see the influence of these variables on both models. The details of the three test cases are shown in table 6.2. The initial kinetic energy is zero in all test cases. In the first test case, the gas has a very low density. As can be seen, both models are in agreement, which is in agreement with the theory. Also, four different levels are visible in the graphs. Let the levels be numbered from one to four, starting on the right. The lowest level is level 1, the second lowest is level 2 etc. According to the analytical solution, the ratio of the pressures at level 1 and level 2, $\frac{p_1}{p_2} = 3.031$. The new CE/SE Van der Waals implementation has $\frac{p_1}{p_2} = 3.030$ in case 1P2, which is a significant improvement over the results obtained in Argrow (1996), which is 3.002. Using the perfect gas law, the ratio is 2.12, so the Van der Waals model is a great improvement for dense gases. Also in case 1P3, the CE/SE scheme results in $\frac{p_1}{p_2} = 3.0293$, which is a slight improvement over 3.028, which is found in Argrow (1996). Also, as expected, the bigger ρ is, the larger is the difference between the perfect gas model and the Van der Waals model, as can be seen in figure 6.2.. Two observations can be made, based on these graphs. First of all, the shock in the Van der Waals gas

Case	δ	CFL	t_{end}	Gases
1P 1	0.4	0.8	0.2	$(\rho, v, p) = \begin{cases} (1,\ 0\ ,1) & 0 \le x \le 0.5 \\ (0.125,\ 0\ ,0.1) & 0.5 < x \le 1 \end{cases}$
1P 2	0.4	0.8	0.02	$(\rho, v, p) = \begin{cases} (0.125,\ 0\ ,10) & 0 \le x \le 0.5 \\ (0.0156,\ 0\ ,1) & 0.5 < x \le 1 \end{cases}$
1P 3	0.4	0.8	0.002	$(\rho, v, p) = \begin{cases} (0.0125,\ 0\ ,100) & 0 \le x \le 0.5 \\ (0.00156,\ 0\ ,10) & 0.5 < x \le 1 \end{cases}$

Table 6.2: The intial conditions for the three cases with different densities

moves slower than the one in the perfect gas. This is due to the lower pressure, compared to the perfect gas law. Secondly, as can be seen in case 1P1, the levels are also not exactly the same. Since the 1D is an intermediate step towards the 2D case, the Sod Shock tube is the only case considered in the comparison between the perfect gas law and the Van der Waals model.

6.2 The two-dimensional case

6.2.1 Validation

For the 2D scheme, two different implementations have been made. The first one uses a structured grid and can be used only for grids with straight borders. The second version is able of capable handling unstructured grids, which opens the door to analyzing much more interesting types of grids. The former is easier to understand and has been implemented as an intermediate step on the way to implementing the latter version. The structured mesh is only used for analyzing the backward step; all the other test cases are implemented using an unstructured mesh. To validate the code, several test cases will be run, namely a backward step, a 30-degree wedge and the NACA-0012 airfoil with 0 and 1-degree angle of attack. A reference solution for the first two test cases can be found in Brown and Argrow (1998) and reference solutions for the last two can be found in Congedo and Cinnella (2007) and Favale and Gadda (2013). The first two make use of the TVD scheme to simulate the flow, and the third one uses the finite volume method.

Backward step

Figure 6.3 shows the plot for three different input conditions. Every time, the left image is the reference solution from Brown and Argrow (1998) and the right one is the plot created by the Van der Waals CE/SE scheme. The ranges of the scales are identical. Since we do not have the numerical data that was used to produce these values, there is no way to do a more precise comparison between the two images. One important observation is that the shock for TD2 in the CE/SE simulation is not perfect, while the shock is perfect in the reference solution. This is most likely due to a lower accuracy of the scheme used to create the reference solution. The initial condition may not be completely accurate, and the CE/SE scheme can capture this imperfection. Besides, the plots seem to visually match very well, which strengthens the belief

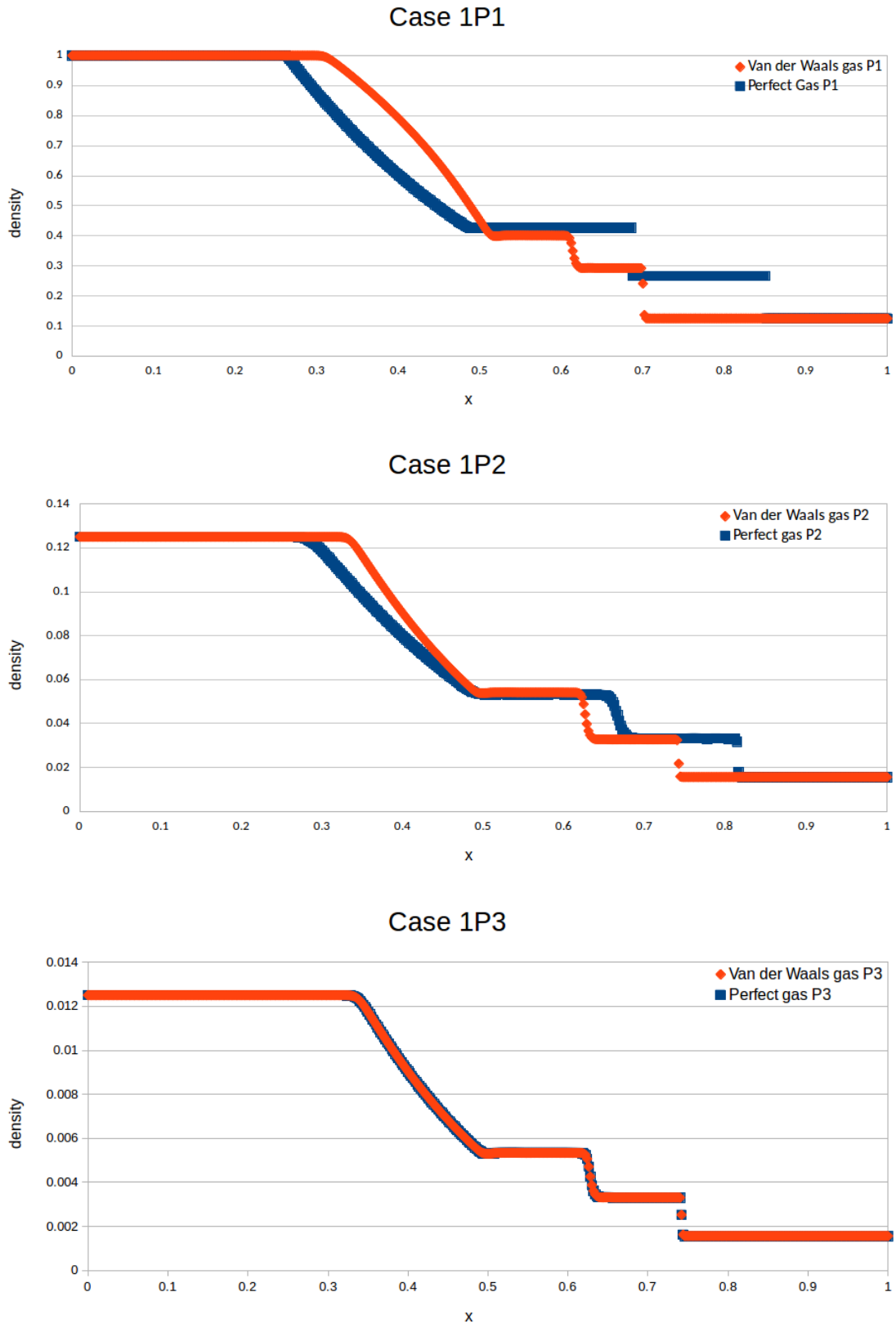

Figure 6.2: The outcome for the perfect gas and the Van der Waals gas for the three different initial states in table 6.2

Case	Inflow				Initial			
	ρ	u_x	u_y	p	ρ	u_x	u_y	p
2D1	0.80	0.14	0.00	0.98	0.56	0.00	0.00	0.89
2D2	0.62	-0.14	0.00	0.98	0.88	0.00	0.00	1.09
2D3	0.85	0.64	0.00	1.01	0.28	0.00	0.00	0.58

Table 6.3: Three initial states for dense gases

that the CE/SE scheme was implemented correctly. The initial states are listed in table 6.3.

30 degree wedge

The second test case is a shock moving against a wedge with an angle of 30 degrees. The results are shown in figure 6.4, in the same order as before. In general, the results seem to match well, however, just as for the backward step, a more precise validation is not possible and therefore, some reservation about the correctness should be called for.

In test case 2D2, for which the results are shown in 6.4a-b, a difference can be observed in the shock. In the reference solution, a single wave front is shown, while in the outcome of the CE/SE scheme, a second discontinuity appears. Most likely, the test case presented in Brown and Argrow (1998) does not result in a perfect shock. The paper was written in 1999, so most likely the computations were not fine enough to observe this difference. To confirm this, the same inflow condition has been set in the 1D code. It is the same test case which also produced a second wavefront in the backward step.

Also at the corner of the edge and the right side of the mesh, some instability occurs. This has to do with the boundary condition, which is known to be not perfect. This can cause inaccuracies at the boundary.

NACA-0012 airfoil, 0 degrees angle of attack

The NACA airfoils are a series of airfoils, in which each airfoil is identified by four numbers. The first number is maximum camber, the second number the position on the wing where the camber is maximum, and the last two digits define the maximum thickness as a percentage of the chord length. The airfoil used in for validation is the NACA-00012 profile, which means that it has no camber and its thickness it 0.12 times its chord length. To create a grid around this airfoil, a C-grid structure is used, as shown in figure 6.5. A reference solution for the NACA-0012 with 0-degree angle of attack can be found in Cinnella and Congedo (2005). The validation will

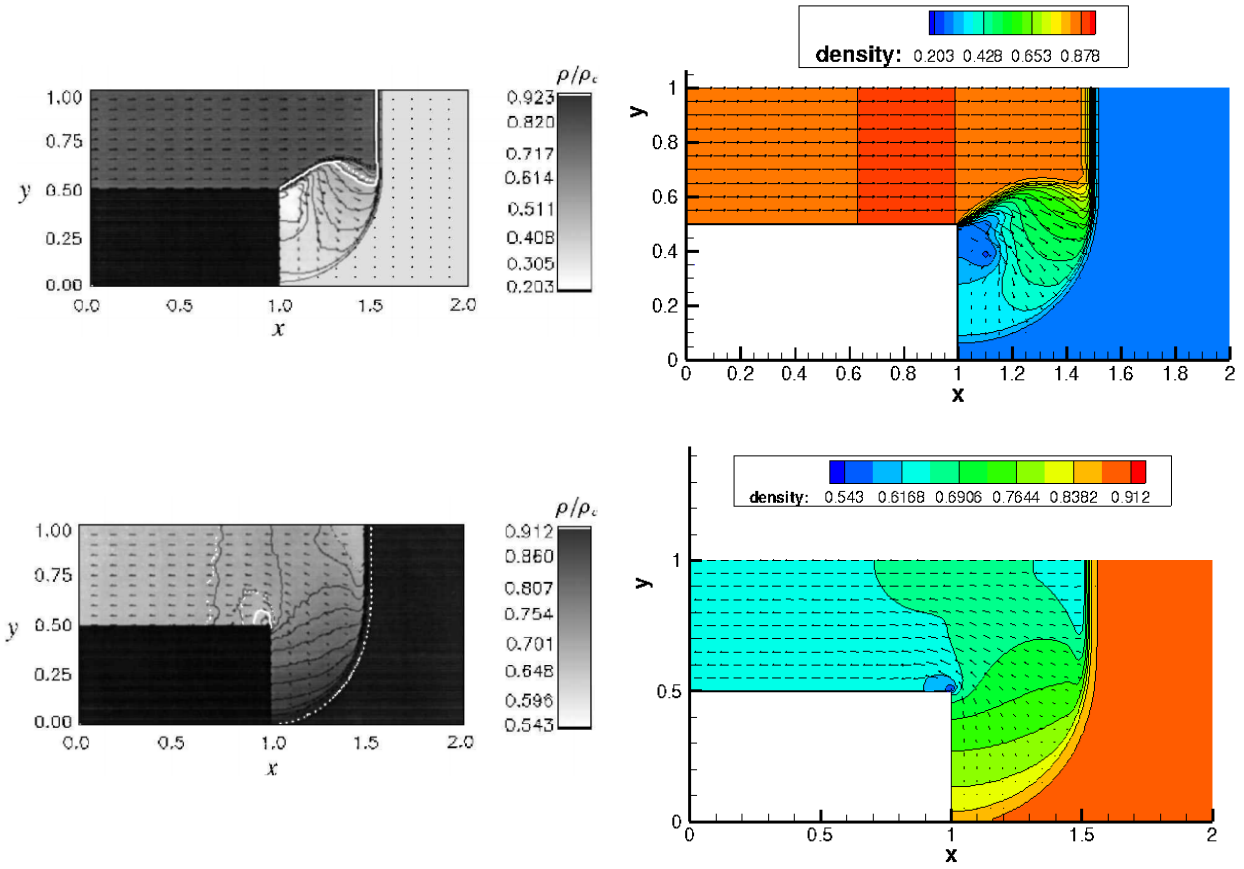

Figure 6.3: Comparison of the data obtained in Brown and Argrow (1998) (left) and obtained by the CE/SE implementation (right) for test case 2D3 and 2D2 respectively

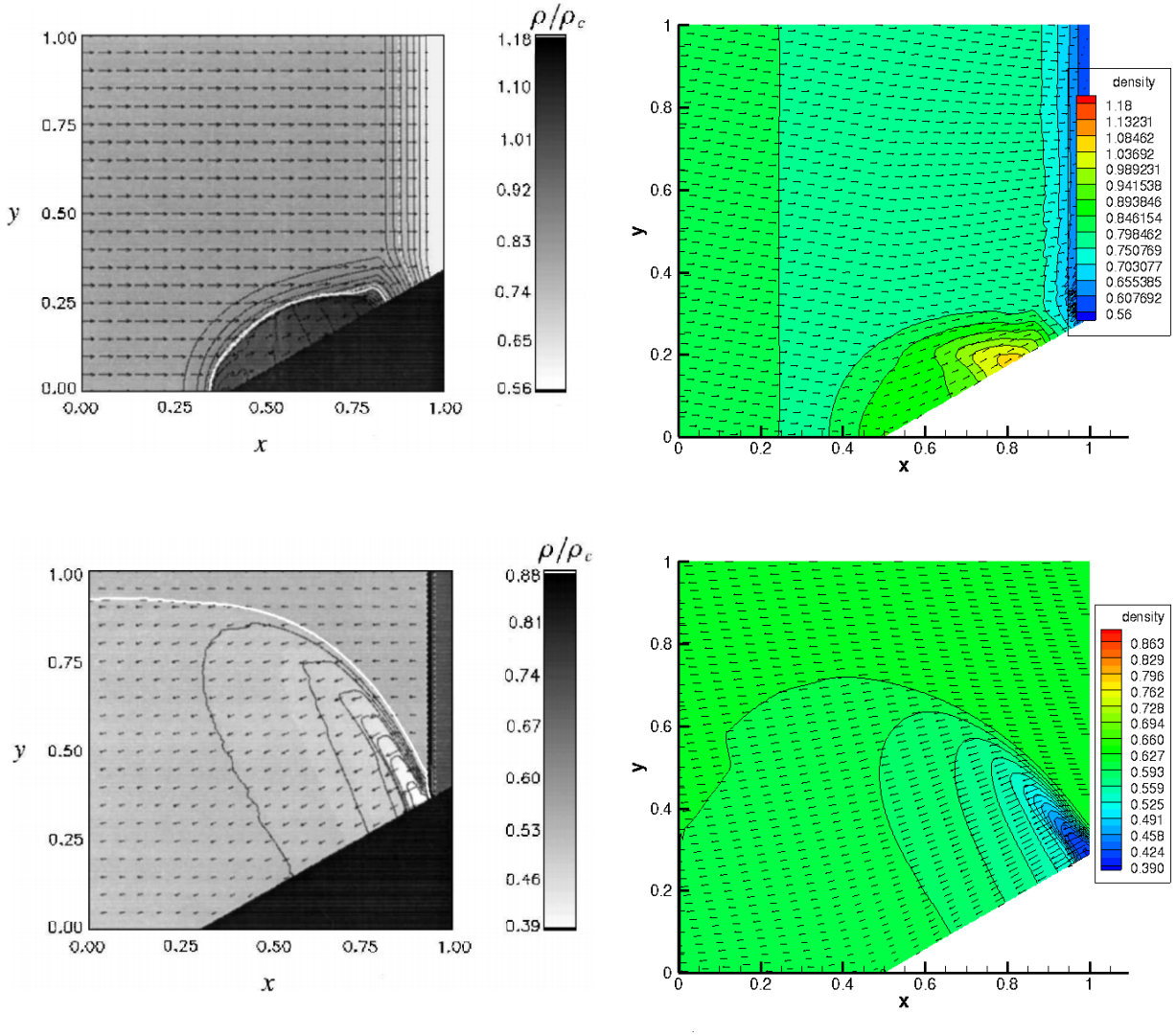

Figure 6.4: Comparison of the data obtained in Brown and Argrow (1998) (left) and obtained by the CE/SE implementation (right) for test case 2D1 and 2D2 respectively

consist of comparing the pressure coefficient, C_p, around the wing profile. Because the wing NACA-0012 wing profile is completely symmetric, the C_p above and below the wing should be equal if the angle is zero degrees. This is true in both the reference solution and the CE/SE implementation, so therefore only one line will be shown in the graph. The result can be found in 6.6. In Favale and Gadda (2013), the initial condition is given by the density, pressure and Mach number. To convert to Mach number to the non-dimensionalized velocity, we have to

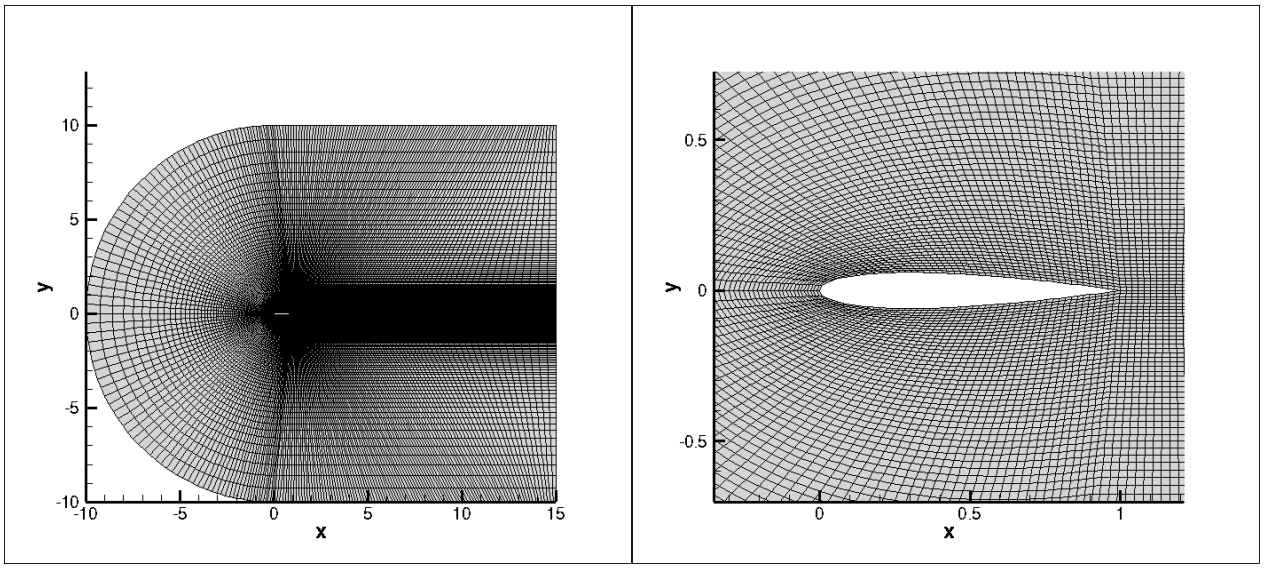

Figure 6.5: The structure of the mesh (a) and zoomed in to show how the mesh is structured around the wing (b)

make use of the definition of the Mach number:

$$M = \frac{\sqrt{u_x^2 + u_y^2}}{a} = \frac{\sqrt{(\cos(\alpha)u_{tot})^2 + (\sin(\alpha)u_{tot})^2}}{a} = \frac{u_{tot}}{a} \tag{6.3}$$

where a is given by equation 3.14, u_{tot} is the total velocity and α is the angle of attack. The flow around the wing profile is shown in figure 6.6b-c and the plot of C_p is given in figure 6.6-a. It can be seen that the C_p profiles do not match. If $\gamma = 1.0125$ is used for the CE/SE scheme, the results do not match the reference solution. However, if $\gamma = 1.4$, the shape of the plot matches the reference solution much better. According to the paper, $\gamma = 1.0125$ in the reference solution. A lot of effort has been put in finding the source of this discrepancy, but no clear explanation has been found. Three differences between the CE/SE Van der Waals implementation and the reference solution have been identified:

- **Equation of state** Congedo and Cinnella (2007) makes use of the MAH equation of state, an EOS for describing dense gasses, which is based on the Van der Waals EOS. This EOS is more precise than the Van der Waals EOS, which might explain why there is a difference between the results in the paper and the Van der Waals CE/SE scheme

- **Boundary condition** As observed in 6.2.1, the boundary condition is not perfect, and

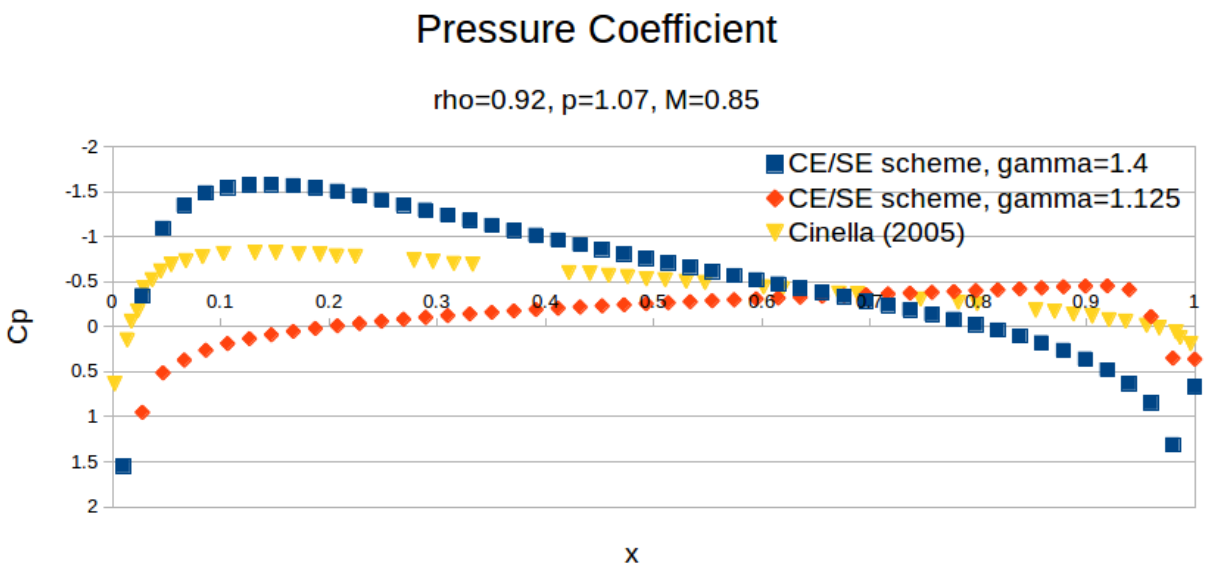

Figure 6.6: The pressure coefficient for test case ($\rho = 0.92, M = 0.85, p = 1.07$)

some unwanted effects may appear near the walls. Therefore, the results around the wing may not be completely correct.

- $\gamma - \delta$ **relation** Most likely, the difference can be explained with investigating the relation between γ and δ. Throughout this thesis, it was used that $\delta = \gamma - 1$. However, a more precise relation, which is based on the Van der Waals model can be used. This relation is derived in Berberan-Santos et al. (2008) and given by:

$$\delta = (\gamma - 1)(1 - \frac{9}{4TV}) \tag{6.4}$$

where V is the volume, which is non-dimensionalized with respect to the critical volume. It can be seen that if TV is very high, this reduces to $\delta = \gamma - 1$. It could be possible that in all the previous test cases T and V were sufficiently high, so that the extra term had almost no influence. Probably, the temperature or the volume decreased so much in the NACA-0012 test case, that the extra term cannot be neglected and might cause the incorrect results. This could explain why the results are completely different for different values for γ and δ. To test this hypothesis, one should compare the minimum temperatures and volumes for the different test cases. Another way to test the theory is replacing $\delta = \gamma - 1$ by equation 6.4

in the implementation. This would require a restructuring of the program, since eq. 6.4 depends on the temperature, which in turn depends on δ. Also, δ must be calculated for each spatial position at every time step. This provides opportunities for further research.

NACA-0012 airfoil, 1-degree angle of attack

Now the inflow is rotated by 1 degree, to generate lift around the wing profile. This results in a lower pressure above than below the wing, which in turn results in a difference between the C_p above the wing and below the wing. The test case that has been examined is equal to the one described in the previous section: $\rho = 0.92, M = 0.85, p = 1.07$. The results are shown in figure 6.7. Just as in the 0-degree case, the C_p profile of the CE/SE implementation does not match the reference solution. However, the difference between $\gamma = 1.4$ and $\gamma = 1.0125$ is more clear in this case. As can be seen, $\gamma = 1.4$ is much more similar to the reference solution than the $\gamma = 1.0125$ case, even though the reference solution uses $\gamma = 1.0125$. Possible causes have been discussed in the 0-degree angle section. The added value of this 1-degree case, is that difference between the values for γ is much more clear.

6.2.2 Analysis of the results

Because the NACA-0012 airfoil simulation did not give good results, this section is limited to the only test case given in Brown and Argrow (1998) for perfect gasses on a backward step. Because of this, this section will be shorter than could be expected.

The available test case consists of a volume filled with a gas with $\rho = 1$ and $p = 1$ and an inflow gas with $\rho = 1.34$, $u_x = 0.4$ and $p = 1.64$. After 0.6 seconds, the situation is as depicted in figure 6.8. The first observation is that the perfect gas moves faster than the Van der Waals gas, just as in the 1D case. Second, the shock behaves differently for a Van der Waals gas and a perfect gas. This is most clearly visible in the plots in figure 6.9. These plots show the density of both the perfect gas and Van der Waals gas at y=0.5. It can be seen that the perfect gas is has a wave with higher density than the influx, while the Van der Waals gas results in a wave with lower density.

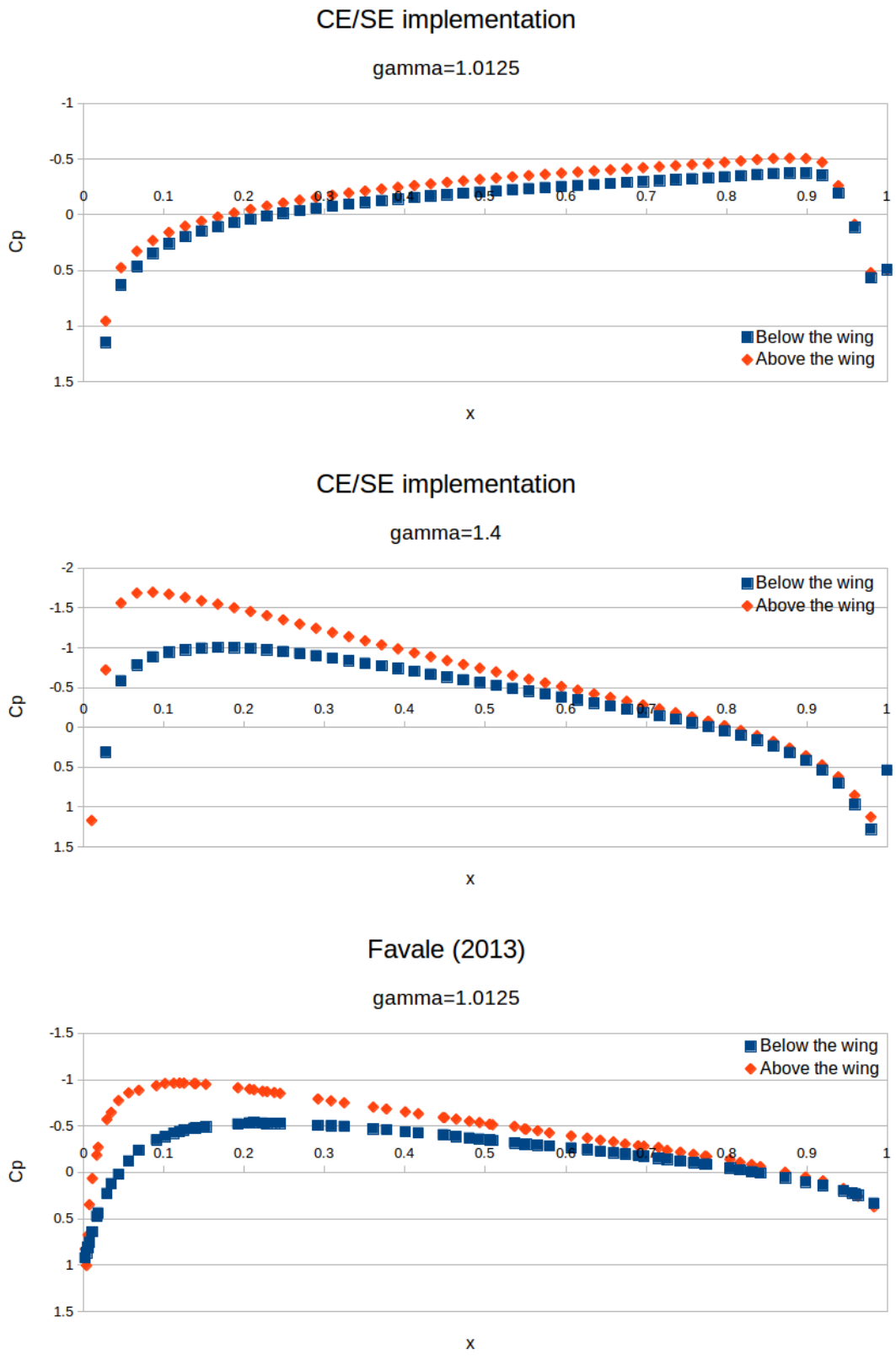

Figure 6.7: Pressure coefficient around the wing for 1 degree angle of attack

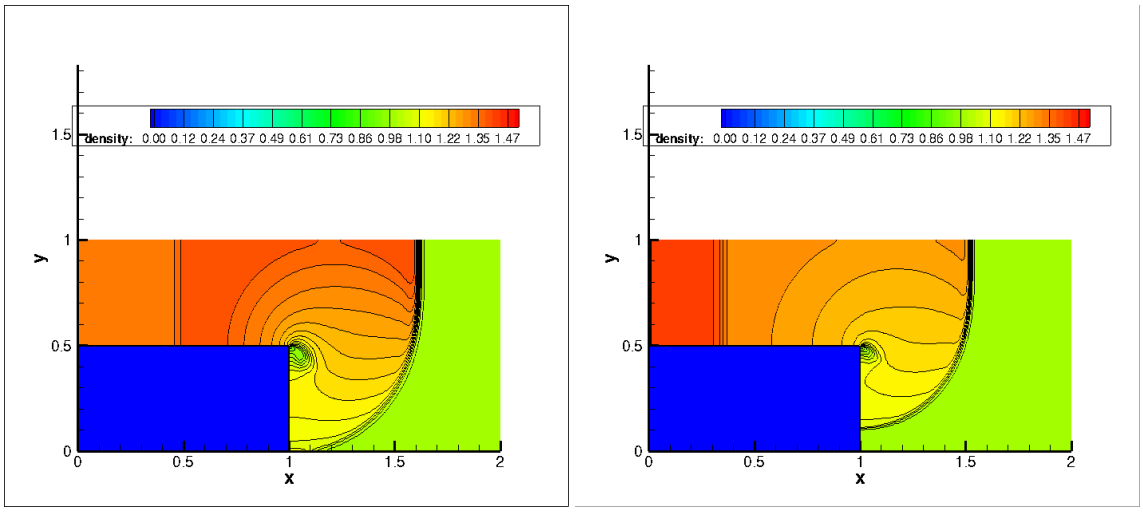

Figure 6.8: The backward step after 0.6 seconds for a perfect gas (left) and a Van der Waals gas (right)

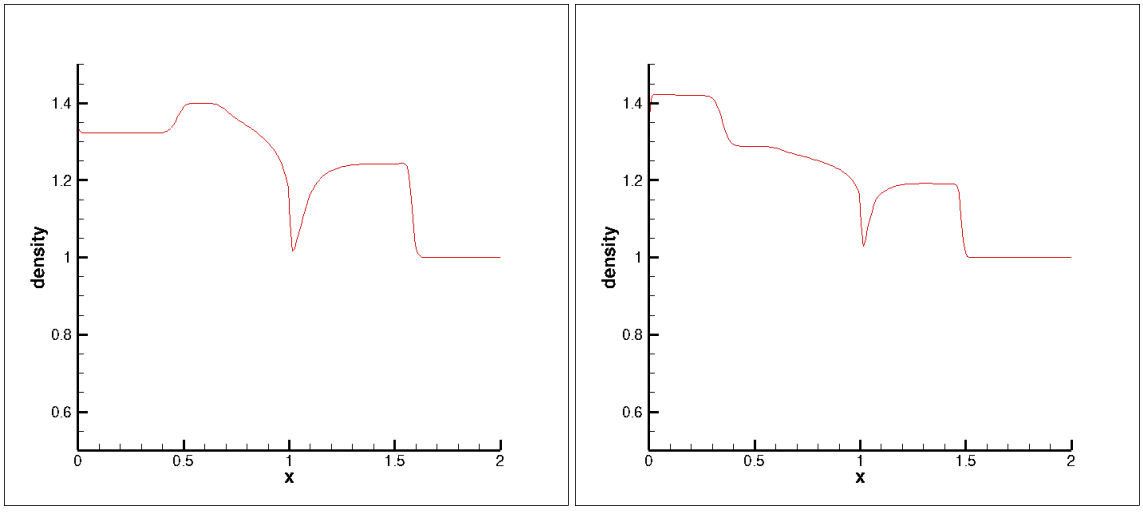

Figure 6.9: The density at y=0.5 for a perfect gas (left) and a Van der Waals gas (right)

7. Summary and Recommendations

7.1 Summary and Conclusions

In the first chapter of this thesis, two objectives were formulated. First, to adapt the CE/SE scheme to use the Van der Waals model instead of the perfect gas law. The second goal was to implement this on a computer and explore the differences between the two models by running simulations. The first objective has been accomplished, and the results are described in chapter 4 and chapter 5. The explanations of the CE/SE scheme heavily depends on the thermodynamic equations, which were derived in chapter 3.

The second goal has partially been achieved. The 1D implementation has been validated, and the differences between the perfect gas model and the Van der Waals model are clearly visible. For dense gases, the Van der Waals CE/SE implementation results in $\frac{p_1}{p_2} = 3.030$, the perfect gas CE/SE scheme results in $\frac{p_1}{p_2} = 2.212$ and Argrow (1996) found $\frac{p_1}{p_2} = 3.002$. According to theory, it the ratio should be 3.031, so the CE/SE scheme is a significant improvement over the method used by Argrow (1996), especially for dense gasses.

The 2D implementation has been successful for structured grids. For unstructured meshes, the outcome of the VdW CE/SE scheme for a wave on the 30-degree wedge matches visually very well with the reference solution. Only, if the same algorithm is used to analyze flow around the wing, it does not produce the right results. A reason for this has not been found. Most likely there is an error somewhere in the code. Probably, the outcome of the test case using the 30-degree wedge is also incorrect, but this could not be observed visually. To detect this possible error, a validated program for simulating Van der Waals flows around simple geometries is needed. This program can be used to produce the numerical data instead of just the images. This validated numerical data can compared to the numerical data produced using the CE/SE Van der Waals implementation to check if the implementation in this thesis is correct.

Therefore, most objectives have been met, only the unstructured mesh around the NACA-0012 profile gives visually invalid results.

7.2 Discussion

The project can roughly be divided into two sections. First of all, the stage where the theory of the Van der Waals CE/SE scheme is derived. All the formulas have been derived by hand and on a computer to minimize the probability of errors. Also, the Van der Waals equations approximate the perfect Gas formulas if the pressure is low, which is to be expected. Therefore, the chances of having errors in this section are relatively low, even more since the 1D version has been validated using computer simulations.
The second stage is the implementation in C(++). During the implementation, two types of errors can occur. First, a typo in a formula or a misplacement of brackets can result in incorrect results and may be hard to detect. Secondly, errors may occur in rounding at the device. The latter is often neglectable, except when extremely high precision is required. The former has a high probability of occurring and a lot of time has been spent searching for bugs. A typo might also be the reason the invalid results of the flow around the NACA-profile. This would imply that the results for the wedge are also invalid, but that the difference is not observable by eye. A final possibility is that the code provided as a starting point contained some error, which had not been observed before. For example, it is known that the boundary condition in the algorithm is not very precise, which may cause incorrect results at a boundary.

7.3 Recommendations for Further Work

Further research should focus on troubleshooting the invalid results of the flow around the NACA-0012 profile. This would mainly consist of debugging the code, implementing the new $\gamma - \delta$ relation and checking the precision of the boundary condition. Once valid results have been obtained, the algorithm can be used to simulate flow around different wing profiles and other angles of attack.
Another way to extend the research of this paper would be to replace the CE/SE Euler solver by

a CE/SE Navier-Stokes solver. Incorporating viscous effects would greatly increase the precision for higher angles of attack. Finally, the Van der Waals model can be replaced by more advanced equation of states, such as the Peng-Robinson EOS. This would increase precision, especially around the critical point, where the Van der Waals model fails to produce good results.

A. Appendix A

A.1 Derivation of a formula for the speed of sound

As described in section 3.3, the speed of sound is given by

$$\bar{a}^2 = \frac{\bar{p}}{\bar{\rho}^2}\left(\frac{\partial \bar{p}}{\partial \bar{e}}\right)_{\bar{\rho}} + \left(\frac{\partial \bar{p}}{\partial \bar{\rho}}\right)_{\bar{e}} \tag{A.1}$$

and the Van der Waals equation of state can be written as:

$$\bar{p} = \frac{\bar{R}\bar{T}\bar{\rho}}{1-\bar{b}\bar{\rho}} - \bar{\alpha}\bar{\rho}^2 \tag{A.2}$$

Plugging A.2 into A.1, gives

$$\frac{\bar{p}}{\bar{\rho}^2} = \frac{\frac{\bar{\rho}\bar{R}\bar{T}}{1-\bar{b}\bar{\rho}} - \bar{\alpha}\bar{\rho}^2}{\bar{\rho}^2} = \frac{\bar{R}\bar{T}}{\bar{\rho}(1-\bar{b}\bar{\rho})} - \bar{\alpha}$$

$$\left(\frac{\partial \bar{p}}{\partial \bar{e}}\right)_{\bar{\rho}} = \frac{\delta\bar{\rho}}{(1-\bar{b}\bar{\rho})} \tag{A.3}$$

$$\begin{aligned}
\left(\frac{\partial \bar{p}}{\partial \bar{\rho}}\right)_{\bar{e}} &= \frac{(\delta\bar{e} + 2\delta\bar{\alpha}\bar{\rho})(1-\bar{b}\bar{\rho}) + b(\bar{\rho}\delta\bar{e} + \delta\bar{\alpha}\bar{\rho}^2)}{(1-\bar{b}\bar{\rho})^2} - 2\bar{\alpha}\bar{\rho} \\
&= \frac{\bar{b}\bar{\rho}\delta(\bar{c}_v\bar{T} - \bar{\alpha}\bar{\rho}) + \bar{b}\delta\bar{\alpha}\bar{\rho}^2 + \delta(\bar{c}_v\bar{T} - \bar{\alpha}\bar{\rho}) + 2\delta\bar{\alpha}\bar{\rho} - \bar{b}\bar{\rho}\delta(\bar{c}_v\bar{T} - \bar{\alpha}\bar{\rho}) - 2\bar{b}\delta\bar{\alpha}\bar{\rho}^2}{(1-\bar{b}\bar{\rho})^2} - 2\bar{\alpha}\bar{\rho} \\
&= \frac{\bar{R}\bar{T} + \delta\bar{\alpha}\bar{\rho} - b\delta\bar{\alpha}\bar{\rho}^2}{(1-\bar{b}\bar{\rho})^2} - 2\bar{\alpha}\bar{\rho} \\
&= \frac{\bar{R}\bar{T}}{(1-\bar{b}\bar{\rho})^2} + \frac{\delta\bar{\alpha}\bar{\rho}}{(1-\bar{b}\bar{\rho})}
\end{aligned} \tag{A.4}$$

This leads to the following dimensional equation for the speed of sound:

$$\begin{aligned}\bar{a}^2 &= (\frac{\bar{R}\bar{T}}{\bar{\rho}(1-\bar{b}\bar{\rho})} - \bar{\alpha})\frac{\delta\bar{\rho}}{(1-\bar{b}\bar{\rho})} + \frac{\bar{R}\bar{T}}{(1-\bar{b}\bar{\rho})^2} + \frac{\delta\bar{\alpha}\bar{\rho}}{(1-\bar{b}\bar{\rho})} - 2\bar{\alpha}\bar{\rho} \\ &= \frac{\delta\bar{R}\bar{T}+\bar{R}\bar{T}}{(1-\bar{b}\bar{\rho})^2} + \frac{\delta\bar{\alpha}\bar{\rho}-\delta\bar{\alpha}\bar{\rho}}{(1-\bar{b}\bar{\rho})} - 2\bar{\alpha}\bar{\rho} \\ &= (1+\delta)\bar{R}\bar{T}\Big(\frac{1}{1-\bar{b}\bar{\rho}}\Big)^2 - 2\bar{\alpha}\bar{\rho} \end{aligned} \tag{A.5}$$

And in non-dimensional form:

$$\begin{aligned} a^2\bar{R}\bar{T}_c &= (1+\delta)\frac{9\bar{R}\bar{T}_c T}{(3-\rho)^2} - 2\alpha\frac{\bar{R}\bar{T}_c}{\bar{\rho_c}}\rho\bar{\rho_c} \\ a^2 &= (1+\delta)\frac{9T}{(3-\rho)^2} - 2\cdot\frac{9}{8}\rho \\ &= \frac{9}{4}\Big[(1+\delta)\frac{4T}{(3-\rho)^2} - \rho)\Big] \end{aligned} \tag{A.6}$$

A.2 The 1D Jacobian matrix for the Euler equation

This section is devoted to deriving the Jacobian matrix $\mathbf{A} = \frac{\partial f_m}{\partial u_k}$, where m and k are 1,2 and 3 respectively and

$$u_1 = \rho \qquad u_2 = \rho v \qquad u_3 = \rho E$$

$$f_1 = \rho v \qquad f_2 = \rho v^2 + Z_c p \qquad f_3 = (\rho E + Z_c p)v$$

Because the equation for p is different for a Van der Waals gas and a perfect gas, both Jacobians will be different and are calculated differently. The matrix for each EOS is given in the next to subsection.

A.2.1 Perfect gas

For a perfect gas, the Jacobian has already been calculated and is given in Chang (1993):

$$\mathbf{A} = \begin{pmatrix} 0 & 1 & 0 \\ -\frac{3-\gamma}{2}\left(\frac{u_2}{u_1}\right)^2 & (3-\gamma)\frac{u_2}{u_1} & \gamma - 1 \\ (\gamma-1)\left(\frac{u_2}{u_1}\right)^3 - \gamma\frac{u_2 u_3}{(u_1)^2} & \gamma\frac{u_3}{u_1} - \frac{3(\gamma-1)}{2}\left(\frac{u_2}{u_1}\right)^2 & \gamma\left(\frac{u_2}{u_1}\right) \end{pmatrix} \tag{A.7}$$

As normal, γ is the constant specific heat ratio $\frac{\bar{c}_p}{\bar{c}_v}$.

A.2.2 Van der Waals gas

The Jacobian for the Van der Waals gas had to be derived explicitly for this project. In order to keep the equations readable, they will refer to the derivative of the pressure and the velocity. These derivatives will be derived first. The pressure is defined by equation 3.13:

$$\begin{aligned} p &= \frac{\rho\delta(8E - 4u^2 + 9\rho)}{3-\rho} - 3\rho^2 \\ &= \frac{u_1\delta(8\frac{u_3}{u_1} - 4\left(\frac{u_2}{u_1}\right)^2 + 9u_1)}{3-u_1} - 3(u_1)^2 \\ &= \frac{\delta(8u_3 - 4\frac{(u_2)^2}{u_1} + 9(u_1)^2)}{3-u_1} - 3(u_1)^2 \end{aligned} \tag{A.8}$$

Therefore,

$$\begin{aligned} \frac{\partial p}{\partial u_1} &= \frac{\delta\left[4\left(\frac{u_2}{u_1}\right)^2 + 18u_1\right]}{(3-u_1)} + \frac{\delta\left[8u_3 - 4\frac{(u_2)^2}{u_1} + 9(u_1)^2\right]}{(3-u_1)^2} - 6u_1 \\ \frac{\partial p}{\partial u_2} &= \frac{\left[-8\delta\frac{u_2}{u_1}\right](3-u_1)}{(3-u_1)^2} = -\frac{8\delta\frac{u_2}{u_1}}{(3-u_1)} \\ \frac{\partial p}{\partial u_2} &= \frac{\left[8\delta\right](3-u_1)}{(3-u_1)^2} = \frac{8\delta}{(3-u_1)} \end{aligned}$$

Using the equations above, we obtain the following values for the Jacobian:

$$\frac{\partial f_1}{\partial u_1} = \frac{\partial u_2}{u_1} = 0 \qquad \frac{\partial f_1}{\partial u_2} = \frac{\partial u_2}{u_2} = 1 \qquad \frac{\partial f_1}{\partial u_3} = \frac{\partial u_2}{u_3} = 0 \tag{A.9}$$

$$\frac{\partial f_2}{\partial u_1} = \frac{\partial (Z_c p + \rho v^2)}{\partial u_1} = Z_c \frac{\partial p}{\partial u_1} - \left(\frac{u_2}{u_1}\right)^2 \tag{A.10}$$

$$\frac{\partial f_2}{\partial u_2} = \frac{\partial (Z_c p + \rho v^2)}{\partial u_2} = Z_c \frac{\partial p}{\partial u_2} + 2\frac{u_2}{u_1} \tag{A.11}$$

$$\frac{\partial f_2}{\partial u_3} = \frac{\partial (Z_c p + \rho v^2)}{\partial u_3} = Z_c \frac{\partial p}{\partial u_3} \tag{A.12}$$

$$\frac{\partial f_3}{\partial u_1} = \frac{\partial \left[(\rho E + Z_c p) v\right]}{\partial u_1} = -\frac{u_3 u_2}{(u_1)^2} + Z_c \left[\frac{\partial p}{\partial u_1}\frac{u_2}{u_1} - p\frac{u_2}{(u_1)^2}\right] \tag{A.13}$$

$$\frac{\partial f_3}{\partial u_2} = \frac{\partial \left[(\rho E + Z_c p) v\right]}{\partial u_2} = u_3 + Z_c \left[\frac{\partial p}{\partial u_2}\frac{u_2}{u_1} + p\frac{1}{u_1}\right] \tag{A.14}$$

$$\frac{\partial f_3}{\partial u_3} = \frac{\partial \left[(\rho E + Z_c p) v\right]}{\partial u_3} = \frac{u_2}{u_1} + Z_c \frac{\partial p}{\partial u_3}\frac{u_2}{u_1} \tag{A.15}$$

The equations A.9 to A.15 form the Jacobian matrix **A** for the Van der Waals Euler equation.

A.3 The 2D Jacobian matrix for the Euler equation

A.3.1 Van der Waals gas

The Jacobians for the Van der Waals Euler equation are given by:

$$\mathbf{A^x} = \begin{pmatrix} 0 & 1 & 0 & 0 \\ -u_x^2 + Z_c p_{u1} & 2u_x + Z_c p_{u2} & Z_c p_{u3} & Z_c p_{u4} \\ -u_x u_y & u_y & u_x & 0 \\ Z_c p_{u1} u_x - \frac{(\rho E + Z_c p) u_x}{\rho} & Z_c p_{u2} u_x - \frac{(\rho E + Z_c p)}{\rho} & (Z_c p_{u3} u_x & (1 + Z_c p_{u4}) u_x \end{pmatrix} \tag{A.16}$$

$$\mathbf{A^y} = \begin{pmatrix} 0 & 0 & 1 & 0 \\ -u_x u_y & u_y & u_x & 0 \\ -u_y^2 + Z_c p_{u1} & Z_c p_{u2} & 2u_y Z_c p_{u3} & Z_c p_{u4} \\ Z_c p_{u1} u_y - \frac{(\rho E + Z_c p) u_y}{\rho} & Z_c p_{u2} u_y - \frac{(\rho E + Z_c p)}{\rho} & (Z_c p_{u3} u_y & (1 + Z_c p_{u4}) u_y \end{pmatrix} \tag{A.17}$$

where

$$p_{u1} = \frac{\delta(4(u_x^2 + u_y^2) + 18\rho) \cdot (3 - \rho) + (\rho\delta(8E - 4(u_x^2 + u_y^2) + 9\rho))}{(3 - \rho)^2} - 6\rho \tag{A.18}$$

$$p_{u2} = \frac{(-8\delta * u_y)(3 - \rho)}{(3 - \rho)^2} \tag{A.19}$$

$$p_{u3} = \frac{(-8\delta * u_x)(3 - \rho)}{(3 - \rho)^2} \tag{A.20}$$

$$p_{u4} = \frac{8\delta(3 - \rho)}{(3 - \rho)^2} \tag{A.21}$$

A.4 Derivation of condition for invertible Jacobian

A.4.1 Perfect gas

From linear algebra, we known that the inverse of a matrix exists if and only if all its eigenvalues are non-zero. Maple (Monagan et al. (2017)) has been used to find the eigenvalues of the Jacobian matrix, as given in A.7. The eigenvalues are:

$$\begin{bmatrix} u \\ u + \frac{\sqrt{4\delta^2\rho E + 4\delta\rho^2 E - 2\delta(\rho u)^2 - 2(\delta\rho u)^2}}{2\rho} \\ u - \frac{\sqrt{4\delta^2\rho E + 4\delta\rho^2 E - 2\delta(\rho u)^2 - 2(\delta\rho u)^2}}{2\rho} \end{bmatrix} = \begin{bmatrix} u \\ u + v \\ u - v \end{bmatrix} \tag{A.22}$$

where

$$\begin{aligned} \nu &= \frac{\sqrt{4\delta^2\rho E + 4\delta\rho^2 E - 2\delta(\rho u)^2 - 2(\delta\rho u)^2}}{2\rho} \\ &= \frac{\sqrt{\delta(\delta+1)(4\rho^2 E - 2(\rho u)^2)}}{2\rho} \\ &= \sqrt{\delta(\delta+1)\left(E - \frac{1}{2}u^2\right)} = a \end{aligned} \tag{A.23}$$

Hence, the eigenvalues of A are u, $u+a$ and $u-a$, from which is follows that the eigenvalues of $[\mathbf{I} - (\mathbf{A}^+)^2]$ are:

$$\begin{bmatrix} 1 - \left(\frac{\Delta t}{\Delta x}u\right)^2 \\ 1 - \left(\frac{\Delta t}{\Delta x}(u+a)\right)^2 \\ 1 - \left(\frac{\Delta t}{\Delta x}(u-a)\right)^2 \end{bmatrix} \tag{A.24}$$

Defining the Courant number C by $C = \frac{u\Delta t}{\Delta x} \leq C_{max}$ (Courant et al. (1967)), all eigenvalues are non-zero iff:

$$C \neq 1 \qquad \wedge \qquad C \pm \frac{\Delta t}{\Delta x}a \neq 1$$

For most explicit solvers, such as the CE/SE scheme, $C_{max} = 1$, so then the condition reduces simply to:

$$C + \frac{\Delta t}{\Delta x}a \leq 1 \tag{A.25}$$

A.4.2 Van der Waals gas

Following the same strategy as above, we calculate the eigenvalues, using Maple:

$$\begin{bmatrix} u \\ u+\nu \\ u-\nu \end{bmatrix} \tag{A.26}$$

with

$$\begin{aligned}
\nu^2 &= \frac{9}{16}\frac{-4(u_1)^5+24(u_1)^4+18\delta^2(u_1)^3+18\delta(u_1)^3-36(u_1)^3+16\delta u_3u_1+16\delta^2u_3u_1-8\delta^2(u_2)^2-8\delta(u_2)^2}{(-3+u_1)^2(u_1)^2} \\
&= \frac{9}{8}\frac{-2(u_1)^3+12(u_1)^2-18(u_1)+\delta(\delta+1)\left(9u_1+8\frac{u_3}{u_1}-4(\frac{u_2}{u_1})^2\right)}{(-3+u_1)^2} \\
&= \frac{9}{8}\frac{-2\rho(-3+\rho)^2+\delta(\delta+1)\left(8\frac{E}{\rho}-4u^2+9\rho\right)}{(-3+\rho)^2} \\
&= \frac{9}{4}\left[\delta(\delta+1)\frac{4T}{(-3+\rho)^2}-\rho\right] = a^2
\end{aligned} \tag{A.27}$$

This is the same result as for the perfect gas, so the rest of the derivation is equal to that for a perfect gas. Therefore we can conclude that $[\mathbf{I}-\mathbf{A}^{+2}]$ is invertible if:

$$C+\frac{\Delta t}{\Delta x}a \leq 1 \tag{A.28}$$

B. Appendix B

B.1 Explanation CE/SE using triangular mesh

This appendix is an continuation of chapter 5, showing the derivation of the CE/SE scheme using triangular meshes. For this purpose, let us define a uniform three dimensional space-time Euclidean space E_3. This space is divided into congruent triangles, with in the center a hollow or a solid dot. The hollow and solid dots are arranged in such a way that a if a dot is hollow, all its neighbors are solid and vice versa, as depicted in figure B.1a and B.1b. The hollow dots represent the mesh point at time step $n = 0$ and the solid dots are mesh points at time step $n = \frac{1}{2}$. In the same way as conservation elements and solution elements were defined in chapter 4, they will be defined in the 2D case. However, the geometry behind this is more complex and requires an extensive explanation to be understandable for the reader. Since the exact dimensions of these elements are not crucial in answering the main question of this thesis, it will not be discussed here. A full description and proof of the geometrical properties of the conservation and solution elements can be found in Chang et al. (1998), chapter 3 and 4. The most important conclusion is that, just as in the 1D case, the boundary of a CE is formed by subsets of two neighboring SEs on the previous time step. This ensures that a mesh point at time step n can be calculated based on its neighboring mesh points at time step $n - \frac{1}{2}$.

Just as before, the function $u_m(x, y, t)$ can be approximated within the SE of mesh point (j, k) at time t by its first-order Taylor expansion, which will be denoted by $u_m^*(x, y, t; j, k, t)$:

$$u_m^*(x, y, t; j, k, t) = (u_m)^n_{(j,k)} + (u_{mx})^n_{(j,k)}(x - x_{(j,k)}) + (u_{my})^n_{(j,k)}(y - y_{(j,k)}) + (u_{mt})^n_{(j,k)}(t - t^n) \quad \text{(B.1)}$$

where $(u_m)^n_{(j,k)}$ is the value of u_m at mesh point (j, k) at time t. $(u_{mx})^n_{(j,k)}$ and $(u_{mx})^n_{(j,k)}$ are the spatial derivatives in the x- and y-direction of u_m at this mesh point. Also, $x_{(j,k)}$, $y_{(j,k)}$ ant t^n are

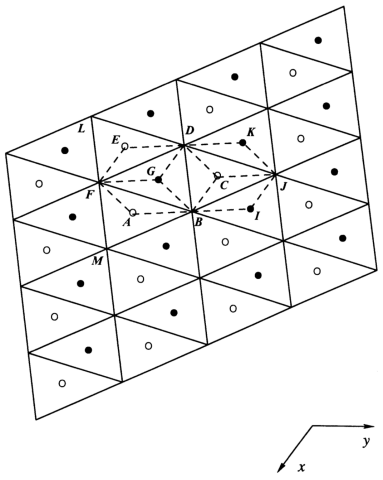

(a) The 2D mesh

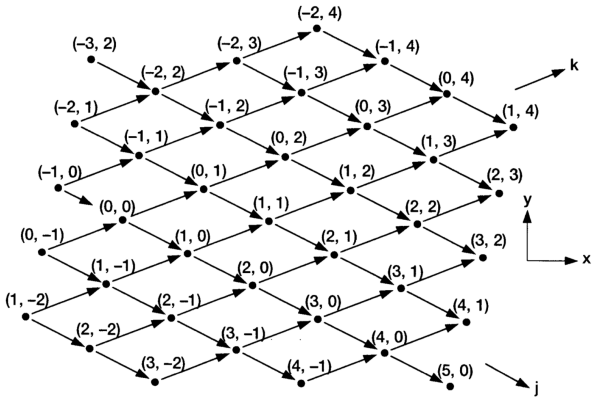

(b) The coordinates of the mesh points at time step $n = \pm\frac{1}{2}, \pm\frac{3}{2}, \pm\frac{5}{2}...$

respectively the x-, y- and time coordinate of (j,k). Using the same notation, can approximate the flux in the x- and y-direction at every point within SE of mesh point (j,k):

$$f_m^{x*}(x,y,t;j,k,t) = (f_m^x)^n_{(j,k)} + (f_{mx}^x)^n_{(j,k)}(x - x_{(j,k)}) + (f_{my}^x)^n_{(j,k)}(y - y_{(j,k)}) + (f_{mt}^x)^n_{(j,k)}(t - t^n) \quad \text{(B.2)}$$

$$f_m^{y*}(x,y,t;j,k,t) = (f_m^y)^n_{(j,k)} + (f_{mx}^y)^n_{(j,k)}(x - x_{(j,k)}) + (f_{my}^y)^n_{(j,k)}(y - y_{(j,k)}) + (f_{mt}^y)^n_{(j,k)}(t - t^n) \quad \text{(B.3)}$$

Here, $(f_m^i)^n_{(j,k)}, (f_{mx}^i)^n_{(j,k)}, (f_{my}^i)^n_{(j,k)}, (f_{mt}^i)^n_{(j,k)}$ are the flux, spatial derivative of the flux in the x- and y-direction and the time derivative, all along the i axis, where $i = x, y$. Hence, we can define $\vec{h}_m^* = \langle f_m^{x*}, f_m^{y*}, u_m^* \rangle$, such that equation 5.1 can be rewritten to:

$$\oint_{S(V)} \vec{h}_m^* \cdot d\vec{s} = 0, \; m = 1,2,3,4 \quad \text{(B.4)}$$

Before evaluating this equation, a new coordinate system will be defined, to recast the results in more convenient forms. As can be seen in figure B.1b, the x-y coordinate system is not the most easy way to describe the mesh points. The new coordinate system consists of two axes ζ and η, such that the coordinates (ζ, η) of any mesh point (j,k,n) are given by

$$\zeta = j \cdot \Delta\zeta \qquad \text{and} \qquad \eta = k \cdot \Delta\eta \quad \text{(B.5)}$$

where $\Delta\zeta$ and $\Delta\eta$ are the mesh intervals in the ζ- and η-directions, respectively. It is shown in Chang et al. (1998) that a transformation matrix T and its inverse T^{-1} exist, such that:

$$\begin{pmatrix} x \\ y \end{pmatrix} = T \begin{pmatrix} \zeta \\ \eta \end{pmatrix} \qquad \text{and} \qquad \begin{pmatrix} \zeta \\ \eta \end{pmatrix} = T^{-1} \begin{pmatrix} x \\ y \end{pmatrix} \tag{B.6}$$

Now, recall the definition of the Jacobian matrix at a mesh point (j,k,n):

$$\left(\mathbf{A}^i\right)^n_{j,k} = \left(\frac{\partial f^i_m}{\partial u_l}\right)^n_{j,k} \text{ where } \ , \ m,l = 1,2,3,4 \tag{B.7}$$

where i is the dimensional space component. Combining equation B.6 and equation B.7 gives:

$$\begin{pmatrix} (\mathbf{A}^\zeta)^n_{j,k} \\ (\mathbf{A}^\eta)^n_{j,k} \end{pmatrix} = T^{-1} \begin{pmatrix} (\mathbf{A}^x)^n_{j,k} \\ (\mathbf{A}^y)^n_{j,k} \end{pmatrix} \qquad \text{and} \qquad \begin{pmatrix} (u_{m\zeta})^n_{j,k} \\ (u_{m\eta})^n_{j,k} \end{pmatrix} = T \begin{pmatrix} (u_{mx})^n_{j,k} \\ (u_{my})^n_{j,k} \end{pmatrix} \tag{B.8}$$

Also, to increase readability, all variables that are associated with the same mesh point, will be stripped from its indices j,k, and n.

Now the integral in equation B.4 can be evaluated. This leads to the following equation, as derived in Appendix C in Chang et al. (1998):

$$\left[\Sigma^{(q)+}_{r1}\vec{u} + \Sigma^{(q)+}_{r2}\frac{\Delta\zeta}{6}\vec{u}_\zeta + \Sigma^{(q)+}_{r3}\frac{\Delta\eta}{6}\vec{u}_\eta\right]^n_{(j,k)} = \left[\Sigma^{(q)-}_{r1}\vec{u} + \Sigma^{(q)-}_{r2}\frac{\Delta\zeta}{6}\vec{u}_\zeta + \Sigma^{(q)-}_{r3}\frac{\Delta\eta}{6}\vec{u}_\eta\right]^{n-\frac{1}{2}}_{(j,k)} \tag{B.9}$$

$$\text{with } \ q = 1,2; \ r = 1,2,3; \ m = 1,2,3,4$$

which, by summing over q and r, leads to:

$$\vec{u}^n_{(j,k)} = \frac{1}{3}\sum_{r=1}^{3}\left[\Sigma^{\pm}_{r1}\vec{u} + \Sigma^{\pm}_{r2}\frac{\Delta\zeta}{6}\vec{u}_\zeta + \Sigma^{\pm}_{r3}\frac{\Delta\eta}{6}\vec{u}_\eta\right]^{n-\frac{1}{2}}_{(j,k;r)}, \quad r = 1,2,3 \tag{B.10}$$

In these equations:

- $\vec{u}, \vec{u}_\zeta$ and $\vec{u}_\eta$ are 4x1 column vectors, formed by $u_m, u_{m\zeta}$ and $u_{m\eta}$ respectively with $m = 1,2,3,4$.

- $\Sigma^{\pm}_{rq}$ with $r,q = 1,2,3$, are the elements of the so-called coefficient matrix:

$$\begin{pmatrix} \mathbf{I} \pm \mathbf{A}^{\zeta+} \pm \mathbf{A}^{\eta+} & \pm(\mathbf{I} \pm \mathbf{A}^{\zeta+} \pm \mathbf{A}^{\eta+})(\mathbf{I} \mp \mathbf{A}^{\zeta+}) & \pm(\mathbf{I} \pm \mathbf{A}^{\zeta+} \pm \mathbf{A}^{\eta+})(\mathbf{I} \mp \mathbf{A}^{\eta+}) \\ \mathbf{I} \mp \mathbf{A}^{\zeta+} & \mp(\mathbf{I} \mp \mathbf{A}^{\zeta+})(2\mathbf{I} \pm \mathbf{A}^{\zeta+}) & \pm(\mathbf{I} \mp \mathbf{A}^{\zeta+})(\mathbf{I} \mp \mathbf{A}^{\eta+}) \\ \mathbf{I} \mp \mathbf{A}^{\eta+} & \pm(\mathbf{I} \mp \mathbf{A}^{\eta+})(\mathbf{I} \mp \mathbf{A}^{\zeta+}) & \mp(\mathbf{I} \mp \mathbf{A}^{\eta+})(2\mathbf{I} \pm \mathbf{A}^{\eta+}) \end{pmatrix} \tag{B.11}$$

- $\mathbf{A}^{\zeta+}$ and $\mathbf{A}^{\eta+}$ denote the normalized values of the matrix $\mathbf{A}$, respectively $\frac{3\Delta t}{2\Delta\zeta}\mathbf{A}^{\zeta}$ and $\frac{3\Delta t}{2\Delta\eta}\mathbf{A}^{\eta}$

- Σ^{-} is used to advance from time step $n \in \mathbb{Z}$ to time step $n+\frac{1}{2}$ and Σ^{+} to to advance from $n+\frac{1}{2}$ to $n+1$. This means that the time every first time step is different from the second time step, which is different from the 1D case, in which both are the same.

In order to find the marching step for u_ζ and u_η, we have to introduce a new vector $\vec{S}^{\pm}_r$:

$$\left(\vec{S}^{\pm}_r\right)^n_j = \left[\left(\mathbf{I}^{(-)} \circ \Sigma^{+}_{r1}\right)^n_{(j,k)}\right]^{-1} \times \left[\Sigma^{\pm}_{r1}\vec{u} + \Sigma^{\pm}_{r2}\frac{\Delta\zeta}{6}\vec{u}_\zeta + \Sigma^{\pm}_{r3}\frac{\Delta\eta}{6}\vec{u}_\eta\right]^{n-\frac{1}{2}}_{(j,k;r)}, \quad r = 1,2,3 \tag{B.12}$$

$$\text{where} \quad \mathbf{I}^{(-)} = \begin{pmatrix} 1 & -1 & -1 \\ 1 & -1 & -1 \\ 1 & -1 & -1 \end{pmatrix}$$

and the symbol $\circ$ denotes the Hadamard product. As shown in Appedix D.3 in Chang et al. (1998), the inverse in B.12 is guaranteed to exist if the CFL number is lower than $\frac{2}{3}$, but numerical studies suggest that it is generally safe to assume existence as long as the CFL number is smaller than 1. Multiplying B.9 from the left with $\left[\left(\mathbf{I}^{(-)} \circ \Sigma^{+}_{r1}\right)^n_{(j,k)}\right]^{-1}$ and rewriting leads to the final four equations of our marching scheme, as shown in Chang et al. (1999). To advance from time step $n \in \mathbb{Z}$ to time step $n+\frac{1}{2}$:

$$\left(\vec{u}^{+}_\zeta\right)^n_{(j,k)} = \frac{2}{\Delta\zeta}\left(\vec{S}^{-}_2 - \vec{S}^{-}_1\right)^n_j \tag{B.13}$$

$$\left(\vec{u}^{+}_\eta\right)^n_{(j,k)} = \frac{2}{\Delta\eta}\left(\vec{S}^{-}_3 - \vec{S}^{-}_1\right)^n_j \tag{B.14}$$

And similarly, to advance from $n+\frac{1}{2}$ with $n \in \mathbb{Z}$ to time step $n+1$, one has to use the following equations:

$$\left(\vec{u}_{\zeta}^{+}\right)_{(j,k)}^{n} = \frac{2}{\Delta\zeta}\left(\vec{S}_1^{+} - \vec{S}_2^{+}\right)_j^n \tag{B.15}$$

$$\left(\vec{u}_{\eta}^{+}\right)_{(j,k)}^{n} = \frac{2}{\Delta\eta}\left(\vec{S}_1^{+} - \vec{S}_3^{+}\right)_j^n \tag{B.16}$$

To conclude, the marching scheme is formed by the two marching steps described above. That is, to advance from $n \in \mathbb{Z}$ to $n+\frac{1}{2}$ one first applies equation B.10 using Σ^{-} and secondly equation B.13 and B.14. Next, to advance from $n+\frac{1}{2}$ to $n+1$, one applies equation B.10 using Σ^{+} and secondly, equation B.15 and B.16.

The basic idea is similar to the one-dimensional CE/SE scheme, but the geometry and algebra is more complex. A more general and extensive explanation of the scheme can be found in Chang et al. (1998), so if the reader needs more background information, he/she can best consult this paper.

Bibliography

Aldo, A. and Argrow, B. (1995). Dense gas flow in minimum length nozzles. *Journal of fluids engineering*, 117(2):270–276.

Argrow, B. (1996). Computational analysis of dense gas shock tube flow. *Shock Waves*, 6(4):241–248.

Arina, R. (2004). Numerical simulation of near-critical fluids. *Applied numerical mathematics*, 51(4):409–426.

Berberan-Santos, M. N., Bodunov, E. N., and Pogliani, L. (2008). The van der waals equation: analytical and approximate solutions. *Journal of Mathematical Chemistry*, 43(4).

Brown, B. P. and Argrow, B. M. (1998). Nonclassical dense gas flows for simple geometries. *AIAA journal*, 36(10):1842–1847.

Chang, S. (1995). The method of space-time conservation element and solution element - a new approach for solving the navier-stokes and euler equations. *Journal of Computational Physics*, 119:295–324.

Chang, S. et al. (1998). Fundamentals of ce/se method. *NASA TM1998-208843, NASA, Cleveland, Ohio*.

Chang, S., Wang, X., and CY, C. (1999). The space-time conservation element and solution element method– a new high resolution and genuinely multidimensional paradigm for solving conservation laws. *Journal of Computational Physics*, 156:89–136.

Chang, S.-C. (1993). New developments in the method of space-time conservation element and solution element: Applications to the euler and navier-stokes equations. NASA Technical Memorandum 106226, https://ntrs.nasa.gov/archive/nasa/casi.ntrs.nasa.gov/19940006467.pdf.

Chena, Y.-Y. et al. (2011). Solvcon: A python-based cfd software framework for hybrid parallelization. *49th AIAA Aerospace Sciences Meeting*.

Cinnella, P. and Congedo, P. M. (2005). Aerodynamic performance of transonic bethe–zel'dovich–thompson flows past an airfoil. *AIAA Journal*, 43:370–378.

Congedo, P. and Cinnella, P. (2007). Airfoil shape optimization for transonic flows of bethe–zel'dovich–thompson fluids. *AIAA Journal*, pages 1303–1316.

Courant, R., Friedrichs, K., and Lewy, H. (1967). On the partial difference equations of mathematical physics. *IBM journal*, 11(2):215–234.

Dullemond, C. and Kuiper, R. (2015). Lecture numerical fluid dynamics. Chapter 1.

Favale, M. and Gadda, A. (2013). A gpu parallelized two fields full potential formulation for real gases. Master's thesis, Politecnico di Milano.

Monagan, M. B., Geddes, K. O., Heal, K. M., Labahn, G., Vorkoetter, S. M., McCarron, J., and DeMarco, P. (2017). *Maple 10 Programming Guide*. Maplesoft, Waterloo ON, Canada.

Shen, H., Wen, C.-Y., and Zhang, D.-L. (2015). A characteristic space–time conservation element and solution element method for conservation laws. *Journal of Computational Physics*, 288:101–118.